Peer-reviewed version available at Sensors 2019, 19, 4435; doi:10.3390/s19204435

Article

On the Noise Complexity in an Optical Motion Capture Facility

Przemysław Skurowski [1]* and Magdalena Pawlyta [1,2]

[1] Institute of Informatics, Silesian University of Technology, Akademicka 16, 44-100 Gliwice, Poland; Przemyslaw.Skurowski@polsl.pl (P.S.); Magdalena.Pawlyta@polsl.pl (M.P.)
[2] Polish-Japanese Academy of Information Technology, Koszykowa 86, 02-008 Warsaw, Poland; mpawlyta@pjwstk.edu.pl
* Correspondence: przemyslaw.skurowski@polsl.pl; Tel.: +48-32-2372151

Abstract: Optical motion capture systems are state-of-the-art in motion acquisition, however as any measurement systems they are not error free – noise is their intrinsic feature. The works so far mostly employ simple noise model, expressing the uncertainty as a simple variance. In the work we prove the existence of several types of noise and demonstrate how to quantify them using Allan variance. For the automated readout of the noise coefficients we solve the multidimensional regression problem using sophisticated metaheuristics in exploration-exploitation scheme. Besides classic types of noise we identified the presence of the correlated noises and periodic distortion in our facility. We had also opportunity to observe the influence of camera failure to the overall performance.

Keywords: motion capture; evaluation; noise modelling; noise color; Allan variance; simulated annealing; ant colony optimization

1. Introduction

Synthesis and analysis of human motion is an active research area having a plurality of applications in biomechanics and entertainment. Contemporary technologies, allow to capture and process the movement (Mocap) with high realism and accuracy, however, they are not error-proof. Various methods were proposed for the motion acquisition, yet the optical motion capture (OMC) technique, based on tracking of retro-reflective markers in IR images is considered as a gold standard in this field of research. It outperforms other techniques and it has been used for verification of the other technologies – inertial [1,2] or optical [3]. OMC is also considered as a reference motion acquisition for the applications of other Mocap technologies in such demanding areas as medical [4–6] or space research [7].

The uncertainty in optical motion capture systems depends on numerous factors, such as type and amount of used cameras, their physical setup, and mounting, marker size, environmental conditions such as air temperature or humidity, camera noise, and quality of the calibration of the motion camera in the motion capture system. Though, almost all these factors can be controlled by re-calibration of the system or ensuring constant environmental conditions, yet the noise present in the cameras is an inevitable factor that cannot be easily neglected or removed.

In this article we characterize the types and levels of noise in three types of Vicon Motion Capture Camera – MX-T40, Bonita10 and Vantage 5, we use Allan variance (AVAR) [8]n which is a handy tool for identification and evaluation of noise types. We propose how to address the non-trivial regression problem of ADEV curve, by matching it with the component functions using

metaheuristics – simulated annealing (SA) and ant colony optimization (ACO). Moreover, thanks to the observed malfunction of one of the devices we were able to demonstrate, that the proposed approach can be used for quite complex cases of correlated and periodic distortions.

The article is organized as follows – in the p. 2 we provide theoretical background and we demonstrate, that simple variance-based noise quantification is not enough and we introduce Allan variance as an alternative; in p. 3 we describe experimental part – laboratory setup and procedure, next it is followed with an algorithm for parameters estimation description and comments on unexpected phenomena observed during the experiment; p. 4 discloses the experimental results and their analysis followed by a discussion of results ; p. 5 summarizes the article and provides ideas for future work.

2. Background

2.1. Previous works

The accuracy and precision in different OMCs were subject to analysis in several works [9–12]. In those works, the most frequently studied OMCs are one of Vicon System (MX, Bonita, and V-series), or OptiTrack system. Regardless of the system used, the authors of these studies agree that the most important factor that influences the data is camera calibration. Camera calibration originates from photogrammetry [13], it relies on positioning the cameras in a virtual 3D space so that they correspond to the cameras positions in the laboratory. This position and several (minimum two) 2D camera projections of markers are used to reconstruct markers in 3D space [14]. The calibration quality is determined using average re-projection error. This is the mean distance between the 2D image of the markers on camera and 3D reconstructions of those markers projected back to the camera's sensor in pixels.

Windolf et al. [10] reported, that performance of OMC strongly depends on their individual setup and that accuracy and precision should be determined for an individual laboratory installation. They tested both accuracy as a root-mean-square (RMS) error from ground truth and precision as a standard deviation of measured positions in four camera Vicon 460 system. As a ground truth they employed custom-built robot mounted L-shaped template. They verified influence of changing the camera setup, calibration volume, marker size and lens filter application. In the best case they report $63 \pm 5 accuracy$µm and 15µm precision.

In another study, Jensenius et al. [12] tested two OMC systems – Optitrack and Qualisys. They used constancy of position as a quality criterion and identified marker position drifting over the time. They measured drifting velocity (in mm/s) and drifting range (in mm) that identifies volume of uncertainty for marker position. They also emphasize role of proper calibration for the performance of OMC, and coverage of the area within calibration procedure.

In the work of Carse et al. [11], three optical 3D motion analysis systems were compared, one of which was a new low-cost system (Optitrack), and two which were considerably more expensive (Vicon 612 and Vicon MX). They used rigid cluster of markers and measured inter-marker distance and its standard deviation (SD) as a quality criterion. They reached SD values between 0.11 - 3.7 mm depending on the OMC system used.

Results confirming high quality position measurement, using Vicon MX with 5 Vicon F-40 cameras, were obtained in the work of Yang et al. [15]. They considered whether the OMC could be used for the subtle bone deformation during exercises – the task required accuracy better than 20µm. As a test template they used markers mounted on the computer numerical controlled (CNC) milling machine having 1 µm spatial resolution. They tested influence of marker size for cameras located very close to the observed, quite small, volume. They confirmed it is possible to achieve the RMSE accuracy and precision to be 1.2–1.8 µm and 1.5–2.5 µm respectively.

Eichelberger et al. [9] investigated the influence of various recording parameters on the accuracy using Vicon Bonita cameras. These are the number of cameras (6, 8 and 10), measurement height (foot, knee and hip) and movement (static and dynamic). All these affected system accuracy significantly.

Another notable works were conducted by Merriaux et al. [16]. They performed two experimental error estimations in 8 Vicon T40 camera OMC for static and dynamic (fast rotating blade) cases. They used two sophisticated robotic templates. In the static case the estimated errors are mean absolute error (MAE) 0.15 mm for accuracy and RMSE of 0.015 mm for precision. In the dynamic case the observed accuracy was larger, yet still satisfying, it achieved values between 0.3mm to <2 mm. They demonstrated also, that it depends on the object velocity and sampling frequency.

Slightly different, yet interesting study on noise [17] involved aquatic OMC based on Vicon T40 cameras, where the scene was a water-filled tank, cameras are located externally in dry locations and the markers made of dedicated reflective tape (SOLAS) are submerged. They demonstrated no significant difference in accuracy and precision due to various mediums in the optical path.

2.2. Simple Preliminary Gaussian Model

Locating markers in a scene is a continuous process occurring frame-by-frame at the requested sampling frequency. The measurement of the location of a marker can be presumed to be an actual location signal plus additive Gaussian white noise, consequently, locating of each marker location is an independent statistical process. One dimensional case, as depicted in Fig. 1, can be described with normal probability density function:

$$loc(M_k) \approx x_k = N\left(\mu_k, \sigma_k\right), \tag{1}$$

where: $loc(M_k)$ denotes actual location of k^{th} marker in a scene. $N(\cdot)$ denotes normal (Gaussian) distribution, which for real location at x_k is estimated as a mean μ_k, and standard deviation σ_k, that (at best) should be common for all the same markers (of a same size).

The typical uncertainty analysis in measurements employs two factors accuracy and precision [18] – the accuracy that describes how close the estimate μ_k is to actual location x_k and describes the systematic error, whereas σ_k reflects the precision of measurement and describes random part of the error.

Extending the estimation of a marker model to the estimation of a length (L) of a bone, it yields a difference of double marker location measurements, hence its probability density function is described:

$$length(x_1, x_2) \approx PDF(L) = |N(\mu_2, \sigma) - N(\mu_1, \sigma)| = N\left(\mu_e, \sigma_e\right), \tag{2}$$

where: $\mu_e = |x_2 - x_1|$ - expected (in common sense) mean value, σ_e - expected standard deviation, which might take different forms, depending on the case:

A. $\sigma_A = \sigma\sqrt{2}$ – for two identical ($\sigma_1 = \sigma_2$), independent variances (covariance $\sigma_{12} = 0$),
B. $\sigma_B = \sqrt{\sigma_1^2 + \sigma_1^2}$ – for two different ($\sigma_1 \neq \sigma_2$), independent variances ($\sigma_{12} = 0$),
C. $\sigma_C = \sqrt{\sigma_1^2 + \sigma_2^2 - 2\sigma_{12}}$ – for two different ($\sigma_1 \neq \sigma_2$), correlated variances ($\sigma_{12} \neq 0$).

In this paragraph, we would like to refer in advance to the experimental part described in p. 3.1-4. Just to introduce it briefly – the recorded model were two markers of a T-frame template, that was laying steadily on the floor for several hours. T-frame (Fig. 7) is a reference rigid tool for calibrating the OMC systems, where markers are mounted permanently in known locations. The location of two markers and their distance (a bone) were measured with three different types of IR cameras. For the detailed description of the experimental setup please refer to the p. 3.

The brief results – markers location and their distance are gathered in Tab. 1. It contains estimated parameters for locations and lengths, we provide also theoretically calculated values for length. These are: locations mean values and their standard deviations, covariance, and correlation

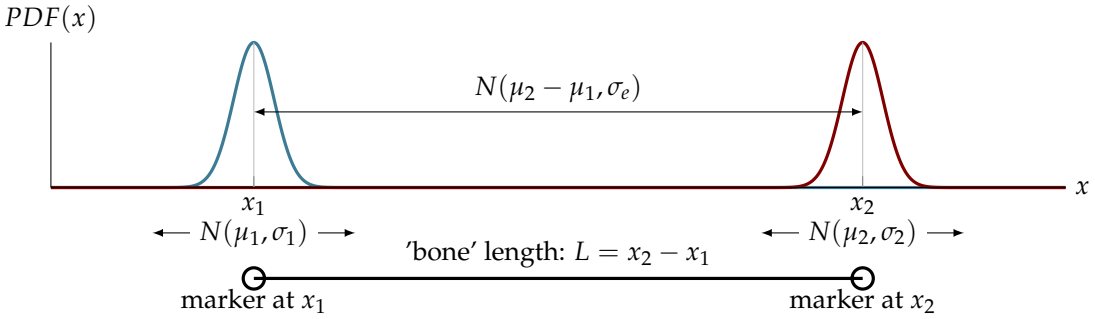

Figure 1. Schematic of situation and corresponding theoretic probability - two markers at x_1 and x_2 identifying a single rigid body (bone) of length l,

(ρ_{12}) as well, furthermore it contains mean value(μ_L) and standard deviation (σ_L) for length as it was reported by the Vicon software. Calculated statistical descriptors are the length (μ_e) and standard deviation in four variants – $\sigma_{A..C}$ as listed above, with two A variants assuming either markers as a potential source of variance value. Figure 2 demonstrates exemplary kernel estimates of location PDFs for one of the camera sets.

Table 1. Stats

	Measured [mm]								Theoretic [mm]				
	μ_1	σ_1	μ_2	σ_2	σ_{12}	ρ_{12}	μ_L	σ_L	μ_e	σ_{A1}	σ_{A2}	σ_B	σ_C
T40	166.5863	0.0217	6.0088	0.0234	0.0004	0.8006	160.5818	0.0143	160.5774	0.0307	0.0331	0.0319	0.0143
Bonita	165.9766	0.1635	5.6644	0.1032	0.0011	0.0670	160.3168	0.1870	160.3121	0.2312	0.1459	0.1933	0.1874
Vantage	166.1736	0.0721	5.7363	0.0942	0.0034	0.4980	160.4388	0.0852	160.4374	0.1020	0.1332	0.1186	0.0855
All	166.4613	0.0157	5.9478	0.0176	0.0001	0.4257	160.5176	0.0178	160.5136	0.0222	0.0249	0.0236	0.0179

Generally, the measurement results conform to the theoretic considerations for correlated random variables – obviously the length measurement results confirmed (not included in the paper) in Chi-squared statistical tests their origin in Gaussian distribution with σ_C. In the considered measurements it is visible in the dispersion of measurements, which is considered as noise. For the low-cost Bonita cameras, the location variance is relatively large, moreover, it is non-correlated to each other (low correlation and covariance), therefore it can be considered as noise. On the other hand, overall dispersion for the high-end T40 cameras is small but highly correlated.

Preprints (www.preprints.org) | NOT PEER-REVIEWED | Posted: 17 September 2019 doi:10.20944/preprints201909.0178.v1

Peer-reviewed version available at Sensors 2019, 19, 4435; doi:10.3390/s19204435

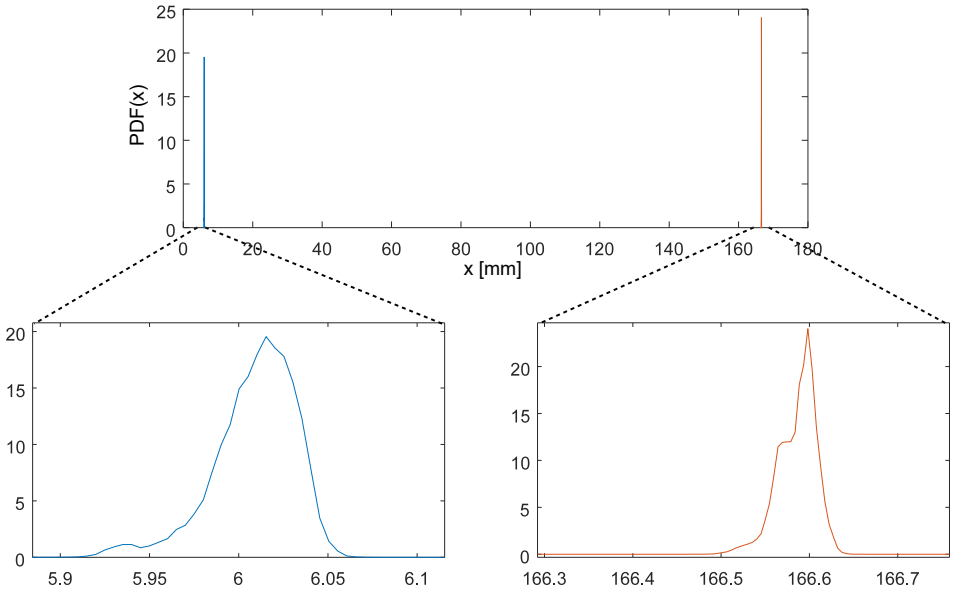

Figure 2. PDF kernel estimation of location for M_1 and M_2 using Vicon T40 cameras

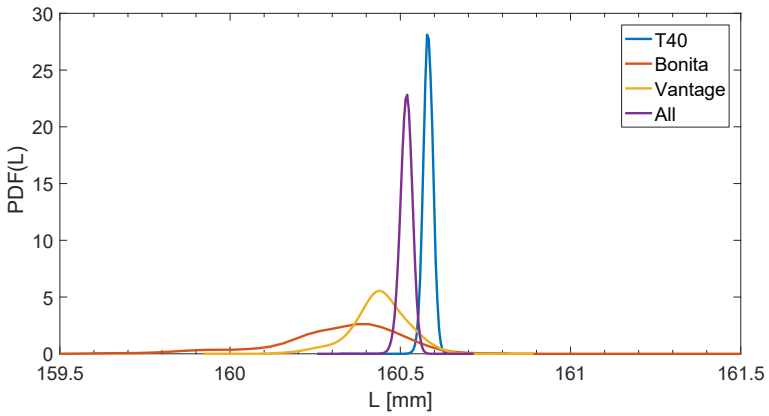

Figure 3. Variable PDF estimation of the same length measurement in OMC with different sets of cameras

The other issue of the error quantification is the lack of reliable ground truth. The Vicon systems return their results with 1/100 mm resolution. It is difficult to obtain a physical template (like the T-frame) manufactured with precision and accuracy comparable or better. For this reason, it is hardly feasible to evaluate the accuracy (bias) of the length estimation with mean values without sophisticated equipment. Fortunately, this aspect is of lesser concern as it describes the systematic error, which is easy to compensate. Moreover, each of the camera sets reports slightly different mean value (see Fig. 3), though the discrepancies between the camera sets are on the level rather satisfactory for the most applications – tenth part of a millimeter.

The number of cameras used for position reconstruction is another factor, that has a significant influence on the uncertainty of measured position – increasing the number of cameras could be considered as an increasing number of measurements. Multiple measurements of the real value reduce an error of measured value, which is described as a standard error calculated based on the standard deviation for observed value:

$$\sigma_{\bar{x}} = \frac{\sigma}{\sqrt{N}}, \tag{3}$$

Preprints (www.preprints.org) | NOT PEER-REVIEWED | Posted: 17 September 2019 doi:10.20944/preprints201909.0178.v1

Peer-reviewed version available at Sensors 2019, 19, 4435; doi:10.3390/s19204435

where: N is a number of observations, σ - standard deviation of observed value. This theoretic, quasi-hyperbolic relationship is depicted in Fig. 4. One can denote clearly visible similarity (with some fluctuations) to the real observed decrease in variations for increasing number of cameras shown in Fig. 5a.

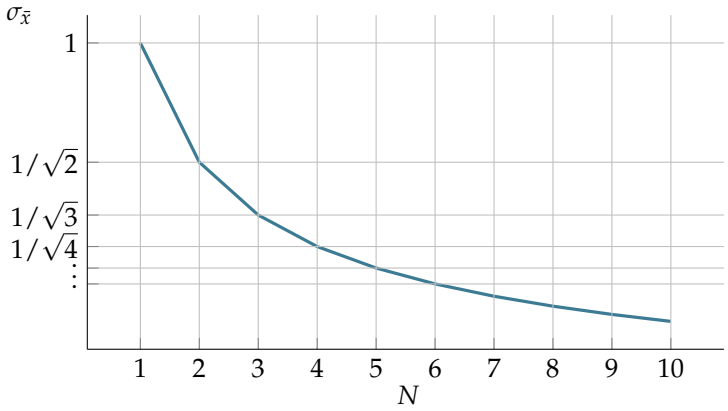

Figure 4. Standard error for estimating actual position with increasing number of measurements

However, as it is depicted in Fig. 5b, the covariance is rather constant regardless of the number of cameras (except very low numbers of cameras), whereas the overall variance decreases as the number of cameras grows. It suggests the presence of a process of unknown origin, that is rather common to the markers and affects their registration then physical devices – e.g. it could be either signal processing or a common mechanic micro trembling of cameras. Hence, according to metrology guidelines [18], if the input quantities are correlated in time, then simple experimental mean or standard deviation might be not enough to describe the uncertainty in the system. In such a situation a dedicated tool, namely Allan variance, is recommended.

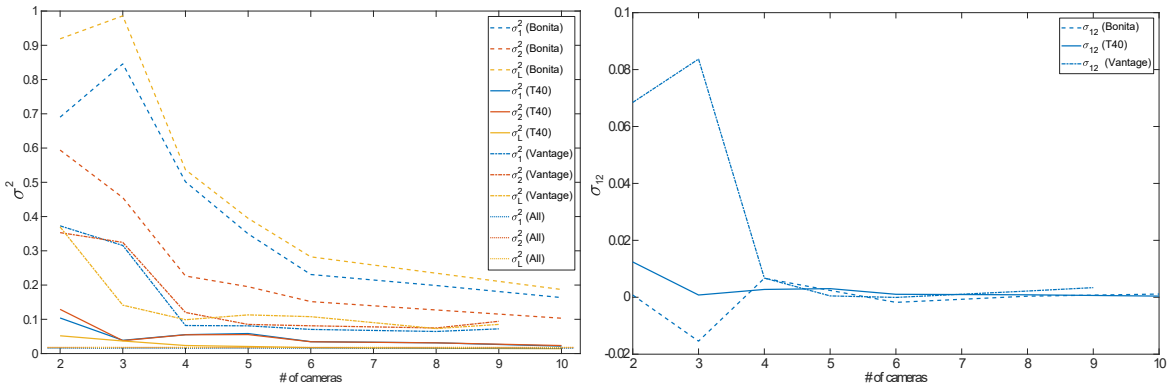

Figure 5. Variances (a) and covariances (b) for variable numbers of cameras of different types

2.3. *Allan variance*

Allan variance (AVAR) a two-sample variance and its square root – Allan deviation (ADEV) are statistical descriptors that were developed for the evaluation of the stability of the time and oscillation in clocks. A notable advantage of this approach that there is no need to provide reference value – ground truth.

Nowadays, the measure is effectively used for quantifying the noises in the measurement of other quantities [19,20], but particularly for inertial motion capture sensors [21,22].

Allan variance [8] is defined as:

$$\sigma_y^2(\tau) = \frac{1}{2}\left\langle (y(t+\tau) - y(t))^2 \right\rangle, \tag{4}$$

where τ is the time intersample spacing, $\langle\cdot\rangle$ denotes expected value.

The AVAR analysis consists of identifying the linear parts of certain slopes of the log-log plot of τ steps versus ADEV (square root of AVAR). It is demonstrated in schematic ADEV plot in Fig. 6. It is a highly beneficial advantage of the AVAR noise quantification over the power spectral density (PSD) – capability not to clutter different noise processes and to precise discriminate several types at once. However, there is also a disadvantage, AVAR is sensitive to the outliers and requires considering outlier cleaning to obtain reliable results.

The conventional types of noise can be identified by their PSD distribution with the power law. The 'color' is given as power relation with respect to frequency ($S(f) \propto 1/f^{\alpha}$). Therefore, overall noise characteristics, comprising different basic noise types are:

$$S(f) = \sum_{\alpha} h_{\alpha} f^{\alpha}. \tag{5}$$

It corresponds to:

$$\sigma_y^2(\tau) \approx \sum_{\tau} h_{\alpha} K_{\alpha} \tau^{\mu}, \tag{6}$$

which for a conventional set of noises yields:

$$\sigma_y^2(\tau) \approx A h_{-2}\tau + B h_{-1} + C h_0 \tau^{-1} + (D h_1 + E h_2)\tau^{-2}. \tag{7}$$

Conventional (color) noise types are gathered in Tab. 2,

Table 2. Power-law noise types and their Allan variance representation

Noise name	α	μ	K_{α}	$\sigma^2(\tau)$
Random walk	-2	1	A=$\frac{2\pi^2}{3}$	$\sigma_r^2(\tau) = \frac{2\pi^2}{3} h_{-2}\tau$
Flicker (pink) noise	-1	0	$B = 2\ln 2$	$\sigma_f^2(\tau) = 2\ln(2) h_{-1}$
White noise	0	-1	$C = \frac{1}{2}$	$\sigma_w^2(\tau) = \frac{1}{2} h_0 \tau^{-1}$
Blue	1	-2	$D = \frac{1.038 + 3\ln w_h \tau}{4\pi^2}$	$\sigma_b^2(\tau) = \frac{1.038 + 3\ln 2\pi f_h \tau}{4\pi^2} h_1 \tau^{-2}$
Violet	2	-2	$E = \frac{3 f_h}{4\pi^2}$	$\sigma_v^2(\tau) = \frac{3 f_h}{4\pi^2} h_2 \tau^{-2}$

where f_h is bandwidth limit for the measurement system. $A..E$ respective scaling factors K_{α}.

Additionally, two complex distortions can be identified using Allan variance – exponentially correlated (Markovian) and sinusoidal. The Markovian noise is visible in the Allan deviation plot as a single 'bump' with slopes $\pm\frac{1}{2}$. Periodic (sinusoidal) distortion is represented in respective plot as a decaying series of bumps with left-sided slope 1 and right side bump series with constant envelope of a slope -1, however, it is the only case, which is more convenient to be observed and to analyze the distortion in Fourier spectral domain.

Correlated noise PSD is given as:

$$S_c(f) = \frac{(q_c T_c)^2}{1 + (2\pi f T_c)^2}, \tag{8}$$

and corresponding Allan variance has a form:

$$\sigma_c^2(\tau) = \frac{(q_c T_c)^2}{\tau}\left(1 - \frac{T_c}{2\tau}\left(3 - 4e^{-\frac{\tau}{T_c}} + e^{-\frac{2\tau}{T_c}}\right)\right) \tag{9}$$

Preprints (www.preprints.org) | NOT PEER-REVIEWED | Posted: 17 September 2019 doi:10.20944/preprints201909.0178.v1

Peer-reviewed version available at Sensors 2019, 19, 4435; doi:10.3390/s19204435

where: q_c is the noise amplitude, T_c is the correlation time.

Sinusoidal noise PSD has a form of two peaks, modeled with Dirac delta:

$$S_s(f) = \frac{1}{2}A_s^2\left(\delta(f - f_0) + \delta(f + f_0)\right), \tag{10}$$

and respective Allan variance form:

$$\sigma_s^2(\tau) = A_s^2\left(\frac{\sin^2(\pi f_0 \tau)}{\pi f_0 \tau}\right), \tag{11}$$

where: A_s is the amplitude, f_0 is the frequency, $\delta(\cdot)$ is Dirac delta peak.

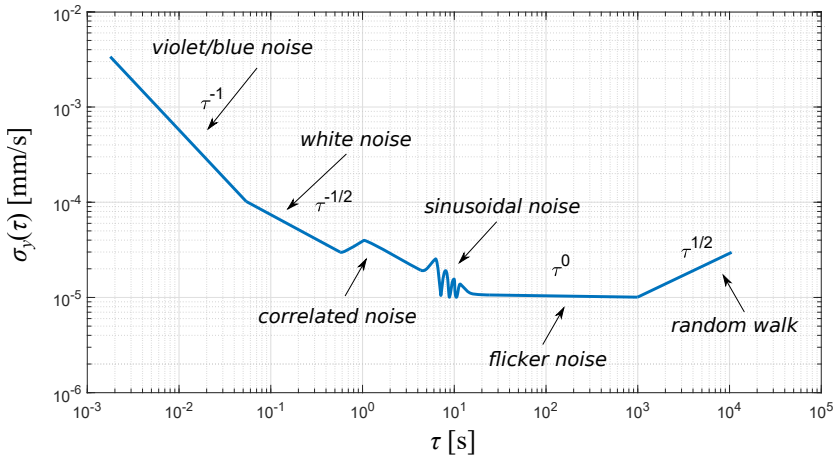

Figure 6. Schematic view on Allan Deviation log-log plot (axis values are for illustrative proposes)

3. Materials and Methods

3.1. Environment

The experimental setup was employed in the Human Motion Laboratory (HML) at the Research and Development Centre of Polish-Japanese Academy of Information Technology in Bytom[1]. Motion system used in this laboratory consists of a total of 30 Vicon Motion cameras of three different types:

- 10 Vicon MX-T40,
- 10 Vicon Bonita10,
- 10 Vicon Vantage V5.

These cameras can record data independently or can be integrated into one larger system with capture volume 9 m x 5 m x 3 m. In order to minimize the impact of external interference like infrared interference from sunlight or vibrations, all windows are permanently darkened and cameras are mounted on scaffolding instead of tripods (as is shown in Fig. 8) The basic information and main differences between used cameras are shown in Table 3.

[1] http://bytom.pja.edu.pl/laboratorium/laboratorium-hml-analizy-ruchu-czlowieka/

Table 3. Vicon camera difference

Camera model	MX-T40	Bonita10	Vantage V5
Resolution [MP]	4	1	5
Max Frame Rate [HZ]	370 @ 4 MP	250 @ 1 MP	420 @ 5 MP
Focal length [mm]	18	4	8.5
Sensor type	CMOS	CMOSIS	CMOS
Type of,LEDs	180 nm NIR	780 nm NIR	850 nm (IR)
Number of LEDs	252	68	22
AOV (HxV)	49.15 x 37.14	70,29 x 70,29	63.5 x 55.1
Dimensions [mm],(HxWxD)	207 x 130 x 75	122 x 80 x 79	166.2 x 125 x 134.1
Weight [kg]	1,8	1	1,6

3.2. Data capture

For the noise analysis needs, a special, nine-hour recording of the two 14 mm markers from the calibration T-frame template (wand) was made. The wand (demonstrated in Fig. 7) was placed in the center of motion capture volume. The three other markers were removed. Data was recorded simultaneously by all the 30 cameras at 120 Hz in standard Vicon software (Vicon Blade version 3.3.1). The XYZ coordinate system was by default oriented according to the T-frame as it is depicted in Fig. 7. Camera calibration was made once with all thirty cameras according to the standard Vicon procedure. The reprojection error for this session, for all the cameras was less than 0.2 pix – mean error for Bonita - 0,1946 pix; Vantage - 0,1891 pix; T40 - 0,1535 pix as reported by the software after the calibration procedure. Additionally, in order to minimize the environmental noise, laboratory technicians were not present in the room during this recording - after the system calibration, all the necessary operations and supervision (start and stop record, system status verification, etc.) were done remotely.

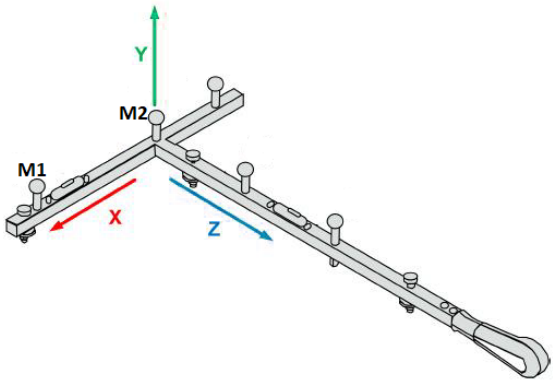

Figure 7. Vicon calibration wand schema (T-frame)

3.3. Data processing

In the post-processing stage in Vicon Blade (Version 3.3.1) software, markers were reconstructed and labeled only, no other filtering or processing was used. This stage was done several times – separately for each camera configuration (including different numbers of cameras of each type). Reconstruction settings were set to the default, for each camera type except the initial set of 2 cameras of each type, where it required to override the demand of marker visibility by three cameras at least. In this trial, the parameter - *'Minimum Cameras to Start Trajectory'* had to be set to 2. All those data were used to create the few datasets, containing several realizations of the same sequence:

- Data set 1: based on all cameras
- Data set 2: based on T40 cameras

- Data set 3: based on Bonita cameras
- Data set 4: based on Vantage cameras

The data sets 2-4 consists of 7 trials, in which a different number of cameras used for 3D markers reconstruction (Table 4). The location of each camera is shown in the Fig. 8. To characterize the noise in different camera type, in all datasets the x,y,z trajectories of both markers and their Euclidean (Eq. 12) distance were analyzed.

$$L = d(M_1, M_2) = \sqrt{(x_1 + x_2)^2 + (y_1 + y_2)^2 + (z_1 + z_2)^2} \tag{12}$$

Table 4. Number and (incrementally) IDs of cameras used for 3D marker reconstruction

Cameras	MX-T40	Bonita10	Vantage V5
2	21,26	2,17	3,4
3	+28	+19	+10
4	+22	+16	+11
5	+27	+18	+7
6	+20	+15	+30
8	+24,29	+13,14	+9,8
ALL	+23,25	+1,12	+5

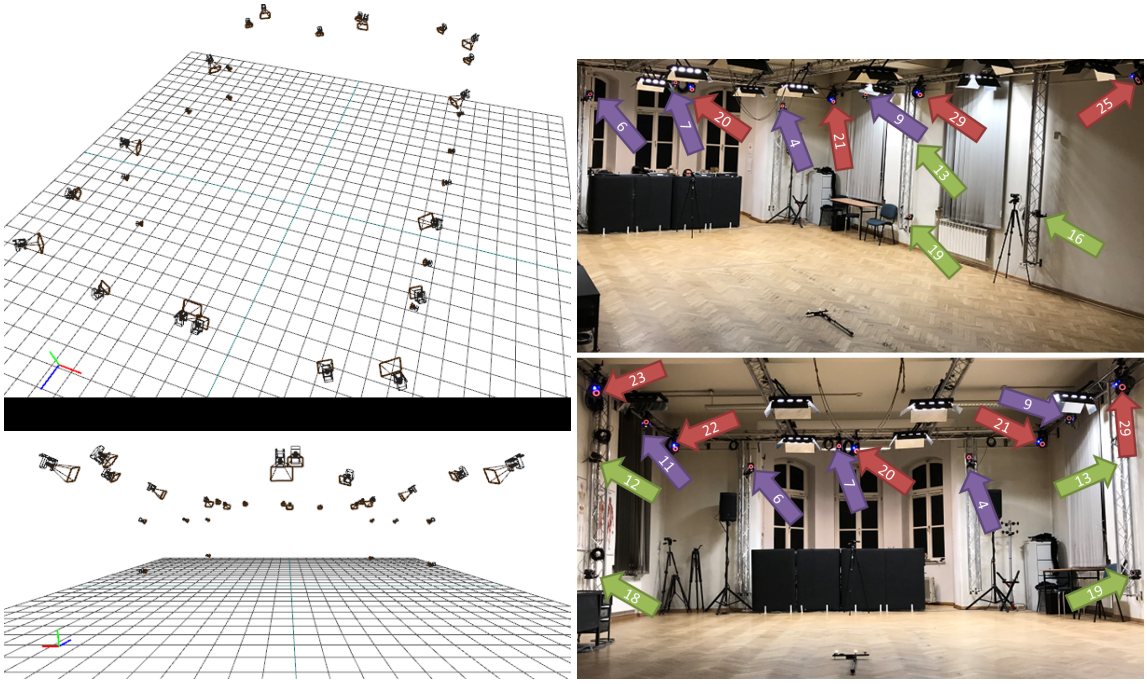

Figure 8. Camera locations: **a**) Schematic view in Vicon Blade software, **b**) actual setup in HML. Color denotes camera series: violet – Vantage, green – Bonita, red – T40

Processing operations in Vicon Blade were limited to 3D reconstruction of marker trajectories and exporting the data to the .c3d file format. Further filtering, analysis, and processing of data were done with Matlab (Version R2016b).

3.4. Noise parameters estimation

For the computing of AVAR from the experimental data we used an implementation by Czerwinski [20]. It implements various AVAR versions, including overlapping estimator, that we chose to use as it is more stable and boundary error prone than conventional one.

Preprints (www.preprints.org) | NOT PEER-REVIEWED | Posted: 17 September 2019 doi:10.20944/preprints201909.0178.v1

Peer-reviewed version available at Sensors 2019, 19, 4435; doi:10.3390/s19204435

The notable advantage of Allan deviation plots is their simple visual interpretation. Moreover, identification of complex – sinusoidal or correlated – distortions is possible just by visual inspection [21] for the presence of bumps in the plot. Another beneficial feature is the ability to estimate the parameters by simple line or poly-line matching to log-log plot [22]. However, straightforward distinguishing between blue and violet noises is not possible in such a case – to obtain these phase dependant noises it would be necessary to employ much slower variant – modified AVAR estimation.

The method for the noise parameters readout from the ADEV curve, used in this research was proposed by Vernotte et al. in [23] – the model employs minimization of weighted least squares (WLS). As it was demonstrated in [19], such an LS model allows even to identify blue and violet noises which are represented jointly by τ^{-2} component.

The weighted LS is represented as following minimization problem that reduces the weighted error between measured AVAR values $\hat{\sigma}_y^2(\tau)$ and a sum of estimated components $\sigma_i^2(\tau)$-s :

$$\hat{H} = \underset{h_{-2},\ldots,h_2,q_c,T_c,A_s,f_o \geq 0}{\arg\min} \left(\sum_{\tau} \left[\frac{1}{\hat{\sigma}_y^2(\tau)} \left(\hat{\sigma}_y^2(\tau) \quad - \sum_{i=\{\substack{v,b,w,\\ f,r,c,s}\}} \sigma_i^2(\tau) \right) \right]^2 \right). \tag{13}$$

Obtaining reasonable results for such a complexand multideimensional non-linear model is a challenging issue. Therefore, we followed roughly a multi-start hybrid algorithm proposed in [24] – multi-start simulated annealing followed by local minimum search, where multiple starts prevent dependence on the initialization. It follows exploration-exploitation scheme, in the first stage simulated annealing (SA), known for avoiding of getting stuck in local minimum, finds solution close to global optimum, which is then refined by local pattern search – for the latter we propose to use ant colony optimization (ACO), specifically the $ACO_{\mathbb{R}}$ variant for continuous domains [25]. Our additional modification is in the initialization stage of the ACO solver, which is at start populated with values jittered around the solution returned by the SA stage. Exemplary regression results are visually demonstrated in Fig. 9, compared with ordinary (non-weighted) LS obtained with Levenberg-Marquardt algorithm.

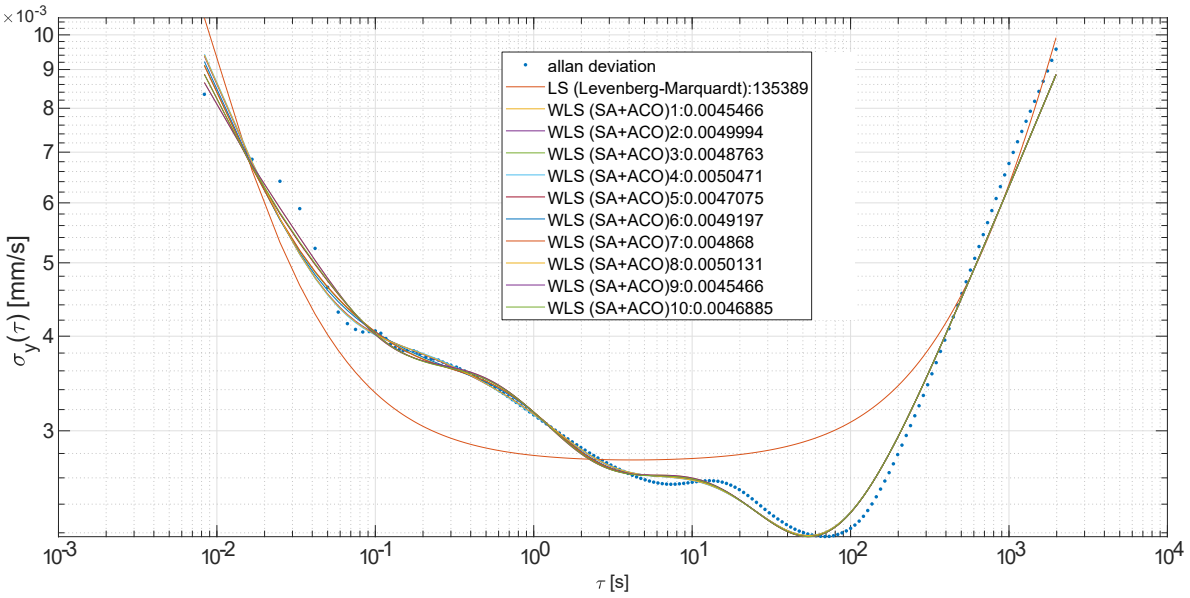

Figure 9. Regression results for an excerpt from the experimental data, demonstrates complex ADEV curve with periodic and correlated components and 10 starts of WLS compared with ordinary LS.

As it was mentioned in the p. 2.3 it is necessary to remove the outliers before the AVAR estimation. For that purpose Hampel filter [26] was employed. It checks the signal whether it is larger than the 3 sigma rule threshold computed robustly on the median absolute deviation (MAD) within a sliding window (in our case 1 second of the past and future values) and replaces outlying values with the local median.

3.5. Remarks on the results

During the data analysis, two issues emerged, its worth to mention them in advance as they could contaminate the results or cause confusion during the interpretation. First, that while recording there occurred a slight seismic crump. The second issue was the failure of one of the cameras (IR LED emitter) during the recording.

The crump can be observed in the trajectories of the markers (Fig. 10a) as a heavy outlier. It has a significant effect on the Allan variance results (see Fig. 10b). That fact draws attention to the need for the careful screening of the measurements for the outliers and proper filtering if necessary – such as the aforementioned Hampel filter.

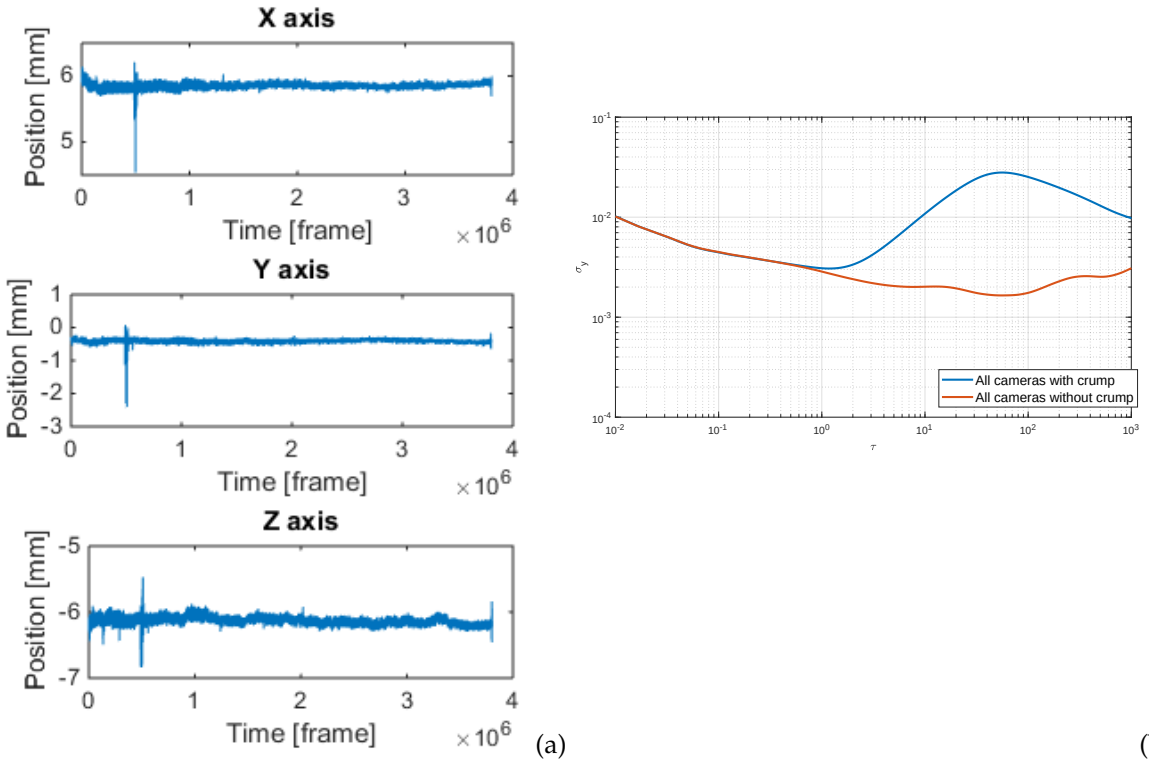

Figure 10. Position X,Y,Z of marker M1 based on data set 1 (**a**) with crump present, (**b**) ADEV of marker distance based on data with and without crump.

The second issue was identified because of the noise levels for data set 4 (Vantage cameras). They were aberrant, for some camera combination the noise levels were increasing when taking more cameras into the reconstruction process. It appeared that one of the cameras was out of order and it would have broken soon after our recordings. Therefore, we excluded it from our analyses and we used up to 9 cameras in the reconstruction for the Vantage data set. Fig. 11 illustrates, how such a

Preprints (www.preprints.org) | NOT PEER-REVIEWED | Posted: 17 September 2019 doi:10.20944/preprints201909.0178.v1

Peer-reviewed version available at Sensors 2019, 19, 4435; doi:10.3390/s19204435

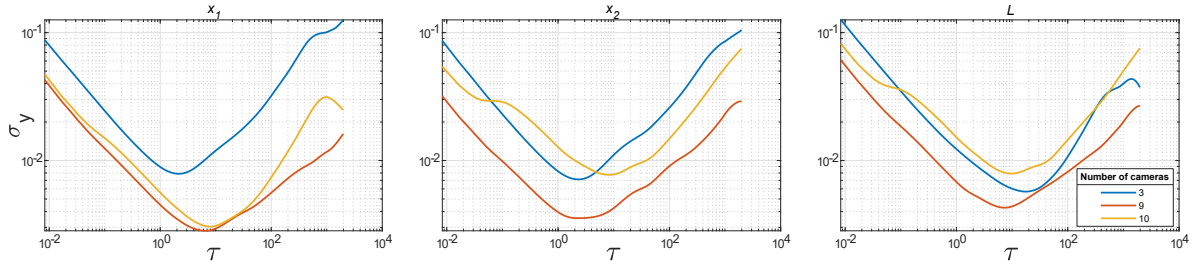

Figure 11. ADEV for Vantage cameras demonstrating the performance loss due to one damaged camera (tenth).

failing device, increases the noise in the results for x dimension – the most contributing to the length (L). It is visible in the figure, that we observe larger ADEV values for 10 cameras than for 9, another noteworthy fact is that markers positions are affected to different extents, and the distance is therefore affected to an intermediate extent. The reason for such an observation remains unclear as the internal details of triangulation in Vicon software are kind of a black box. We suspect the inner quality control procedure, that could, for example, select just some subset of cameras.

There were also indirect consequences of the failing camera. We could observe slight cross-talk of distortions to the other cameras mounted at similar heights (Vantage and T40), resulting in the presence of short term correlated noise (verified in p 4.5). Fortunately-or-not it resulted finally in much more complex ADEV curves we had to analyze, proving that the proposed method is capable to adapt to all the noise types known from the Allan variance literature. The exeplary ADEV curve, obtained for the data after changing the failing camera is included in Appendix B for comparison. It demonstrates ADEV of the whole system in the facility free of the distortions caused the failing IR LEDs.

4. Results and discussion

4.1. Overview

Using the single long sequence recorded with a regime as described in sections 3.1-3.3, we have obtained a pool of sequences obtained with different camera sets. The results were analyzed with an overlapping Allan variance estimator. These results are grouped by camera type and presented as families of Allan deviation plots in Fig. 12 with a varying number of cameras used in the process.

Next, Allan variance noise component parameters were estimated with the procedure described in p. 3.4. The presence and number of correlated and periodic components were examined visually, the verification, whether they are not coming from the periodic distortion, was done by examination of the PSD estimator. The noise parameter estimation results are demonstrated in Figs. 14 and 15, in logarithmic and linear scales to adapt to large range of values. Numerical values are attached in Appendix A in Tables A1–A3.

Finally, the less conventional noises were considered in p. 4.5. These are multiple occurrences of correlated noise and periodic distortion.

4.2. Overall ADEV characteristics

Overall ADEV characteristics for all camera types – T40, Bonita and Vantage are shown in Fig. 12. They reveal that the σ_y values gradually decrease with the increasing number of cameras, however, there are some 'drops' along the camera number axis. That suggest, that certain camera setup is notably better suited for the recorded object – these setups are: 3 cameras for T40, 5 cameras for Bonita, and 4 cameras for Vantage.

Another interesting observation in the overall plots can be denoted when analyzing ADEV plots for measured values along the temporal axis. The σ_y values for the distance L are larger than for the

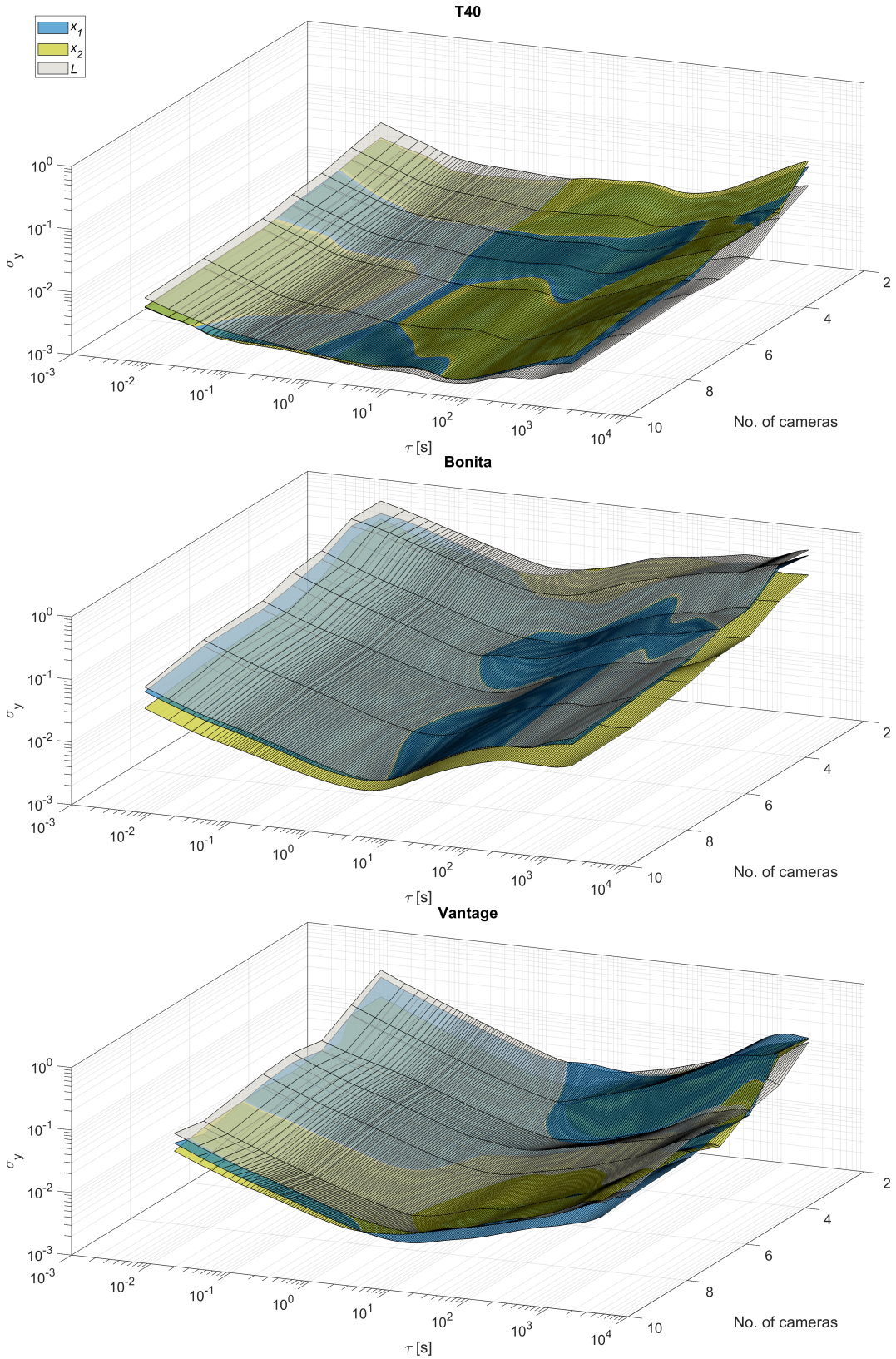

Figure 12. ADEV versus time plots for varying number of cameras (2..max) for three camera types, listed top-down: T40, Bonita, Vantage

Preprints (www.preprints.org) | NOT PEER-REVIEWED | Posted: 17 September 2019 doi:10.20944/preprints201909.0178.v1

Peer-reviewed version available at Sensors 2019, 19, 4435; doi:10.3390/s19204435

contributing locations x_1 and x_2 within the range of short-time noises $\tau \approx 10^{-2} \ldots 10^{1}$, although for the longer time ranges these values are on par or even ADEV values are smaller for the distance than for contributing locations. Apparently, flicker and random walk noises do not add in the system.

We can also observe all the slopes (-1, -1/2, 0, 1/2) from the Tab. 2 in the characteristics plots. The presence of random walk could be a bit confusing at first, if we omit the results of Jensenius [12], one could expect such distortion not to appear. The triangulation process is done frame-by-frame in the system, therefore the position of a marker should be steady, with flicker, white and higher frequency color noises present. However, there might be implicit denoising present in the system done by low pass filtering, such filters act as integrators, therefore they could introduce some low-frequency noises from the higher noise components.

4.3. Comparing the camera types

The logical corollary of results demonstrated in the previous paragraph is a direct comparison of camera types. In Fig. 13 we demonstrate the ADEV plots for each of the camera types at its maximum performance configuration (all cameras). It shows length (L) and marker positions in x as the most important dimension. Comparing the camera types by visual plot inspection confirms the expected outcome, that low-cost Bonita cameras have much higher ADEV values (are more noise affected) than two other camera types. However, ADEV values of up-to-date Vantage cameras indicate that they are more noise affected than relatively old T40s.

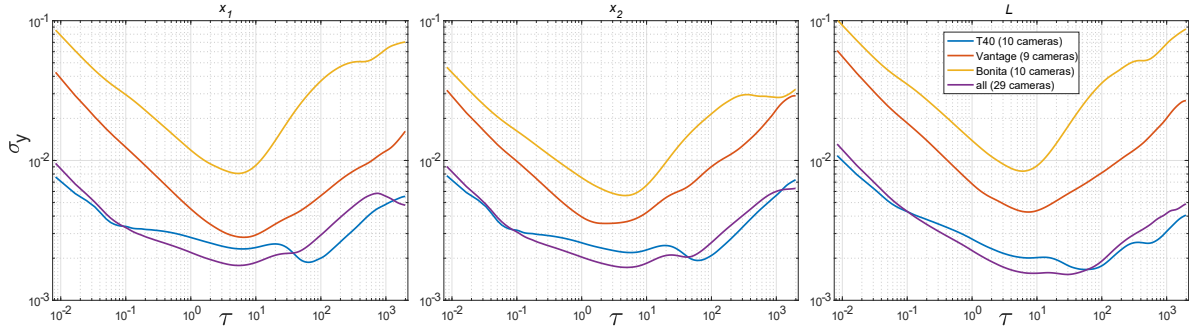

Figure 13. ADEV for maximal numbers of cameras of each type separately and altogether.

4.4. Estimation of basic noise coefficients

Several remarks on the noise colors present in the system, that are based on the noise estimated coefficients (Figs. 14 and 15):

- Random walk and white noise diminishing with the increasing number of cameras, roughly follow quasi-hyperbolic characteristics described with Eq. 3, $h \approx 10^{-5}$
- Flicker and blue noise levels orders of magnitude are relatively constant with low-moderate values $h \approx 10^{-10}$
- Violet noise levels are negligibly small $h \approx 10^{-20}..10^{-300}$

We could also observe intense peak fluctuations in plots of h coefficient characteristics. They could originate from two potential sources – numerical errors in the optimization process, and/or very specific camera geometric configuration, that could improve or degrade the results. However, the general rule (Eq. 3) of decreasing uncertainty with an increasing number of measurements could be observed to some extent for all the noise coefficients (h), but violet one, where it rather seems to be random fluctuations.

4.5. Unconventional distortions

Regarding the less conventional, correlated noises, a series of interesting observation relates to their presence. In Fig. 16a one can observe, that they are mostly independent of the number of

Preprints (www.preprints.org) | NOT PEER-REVIEWED | Posted: 17 September 2019 doi:10.20944/preprints201909.0178.v1

Peer-reviewed version available at Sensors 2019, 19, 4435; doi:10.3390/s19204435

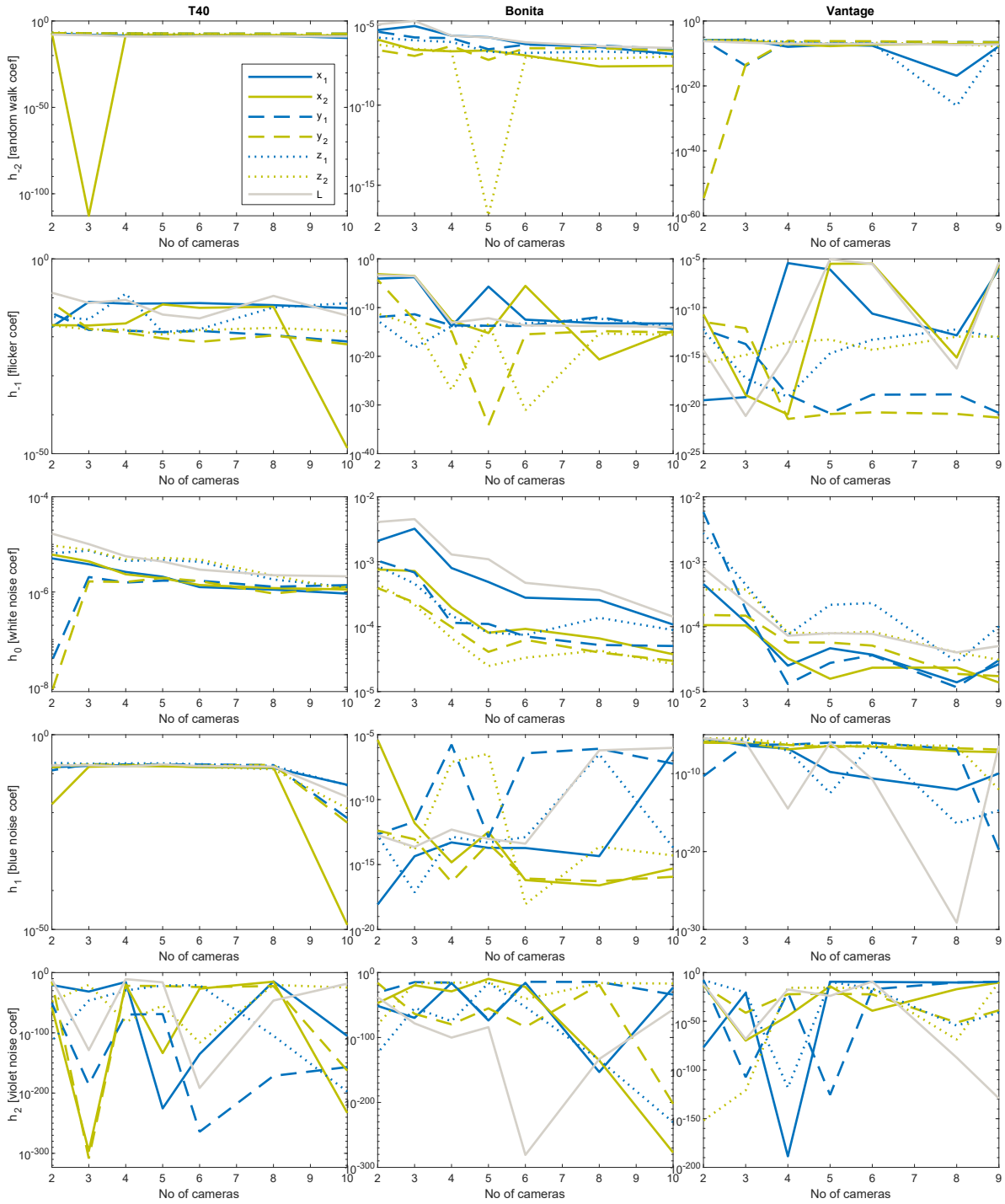

Figure 14. Color noises ($h_{-2}..h_2$) coefficients in logarithmic scale; in columns left to right: T40, Bonita, Vantage

Preprints (www.preprints.org) | NOT PEER-REVIEWED | Posted: 17 September 2019 doi:10.20944/preprints201909.0178.v1

Peer-reviewed version available at Sensors 2019, 19, 4435; doi:10.3390/s19204435

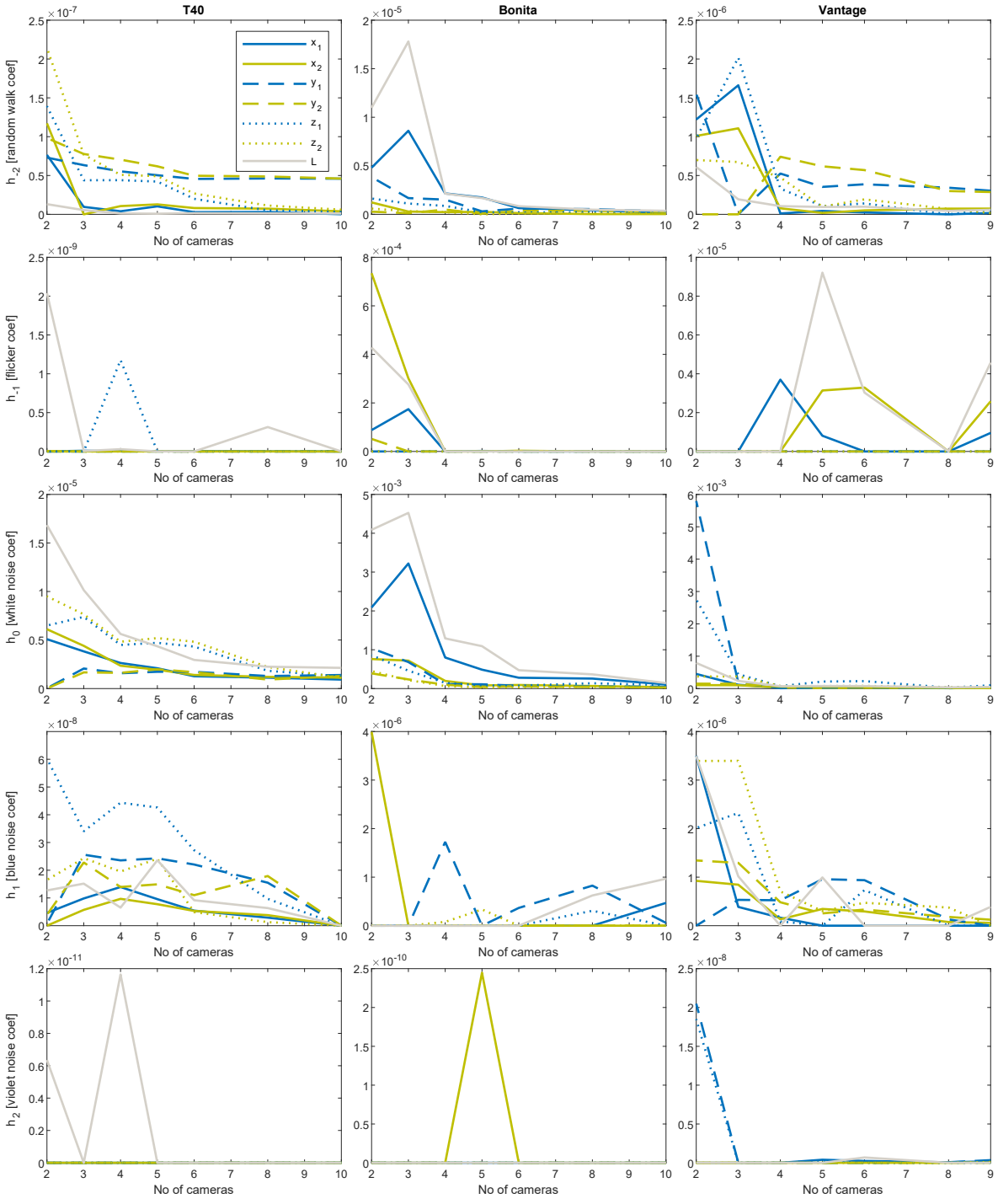

Figure 15. Color noises ($h_{-2}..h_2$) coefficients in linear scale; in columns left to right: T40, Bonita, Vantage

Preprints (www.preprints.org) | NOT PEER-REVIEWED | Posted: 17 September 2019 doi:10.20944/preprints201909.0178.v1

Peer-reviewed version available at Sensors 2019, 19, 4435; doi:10.3390/s19204435

cameras – T_c and q_c parameters remain relatively constant. Moreover, one could note from Fig. 16b, that for correlated noises in the system the longer the time constant the lower amplitude. We could also identify three correlated noise 'classes' of a different correlation time constants. Their sources remain unknown, however, at least we could speculate about their origins based on T_c. Removing the failed camera made the first two of them (see App. B) disappear. Hence our guesses are:

- $10^{-2} - 10^{0}s$ – due to failed camera, though we considered signal processing based first,
- $10^{0} - 10^{1}s$ – due to failed camera, at first we suspected mechanical based microtrembling of camera support,
- $10^{2} - 10^{3}s$ – environmental based such as changes in room temperature.

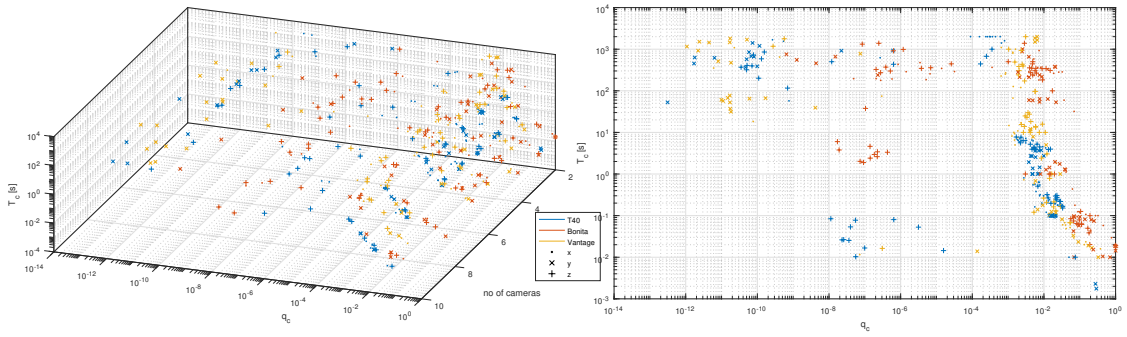

Figure 16. Distribution of correlated noises q_c versus T_c.

Finally, the occurrences of periodic noise of $f_0 \approx 15$Hz frequency had to be checked as it was an unexpected outcome. The verification was done using Welch estimator of PSD (see Fig. 17), and it is present in each of the reconstructions using T40 and Vantage cameras. However, it is usually negligibly small phenomenon, barely observable in most of ADEV plots. Its origin cannot be connected with a recording of any specific camera, but since all the cameras were recording concurrently, it is probably due to some environmental source. Cameras appeared sensitive to a different extent, surprisingly vertical dimensions obtained from the T40 cameras were the most sensitive to this distortion. In case of the Vantage or Bonita cameras it is negligibly small. It requires very large zoom to observe appearance of respective bumps in either PSD or ADEV plots.

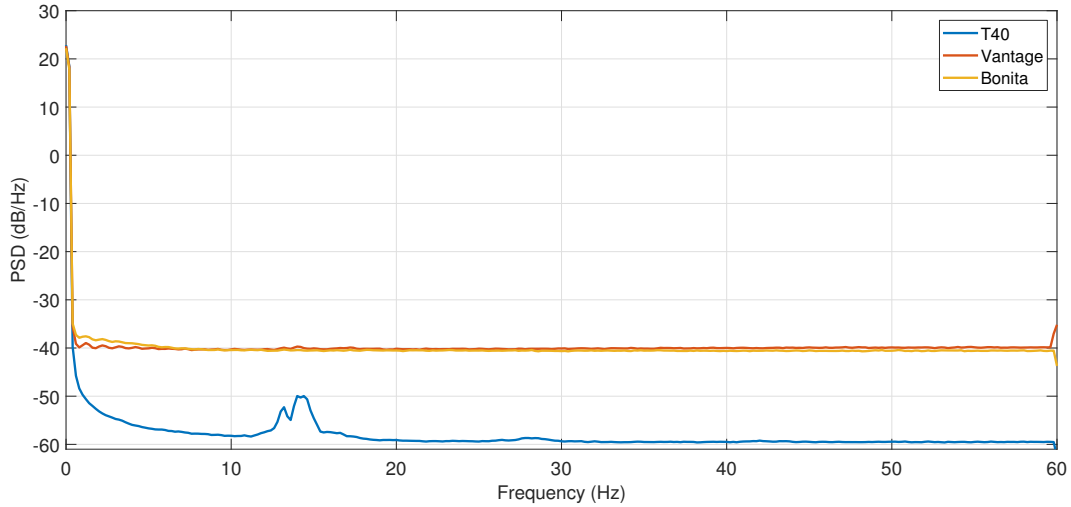

Figure 17. Exemplary verification of periodic distortion using PSD for z_1 reconstructed with maximal number of devices for each camera type

5. Summary

In the article, we demonstrated how to evaluate with Allan variance a compound structure of noise present in the optical Mocap system. The proposed tool was invented for situations when the reliable ground truth is inaccessible. We demonstrated, that it provides outcomes convenient for visual inspection to identify qualitatively noise types actually present in the system or to compare two systems. We have also demonstrated how to employ sophisticated solvers to read the noise parameters from the characteristic ADEV curve, even when it gets quite complicated form.

For our facility, we proved that the main contribution to the imprecision comes from the random walk and white noise, whereas flicker noise and blue noise contributions are several orders of magnitude smaller. The influence of violet noise is negligibly small. We have identified also the presence of quite a long term (tens of minutes) correlated noise, probably due to environmental influence. The registration of the noise connected with camera failure was an additional and unforeseen outcome.

Future works might include extending the basic approach by analysis of AVAR for bone orientation, though it would require preparing quaternionic AVAR. Other interesting aspects are the variability of AVAR depending on the location in the scene, or how much the results are affected by the presence and activities of staff in the lab. The experiments could be also repeated in different Mocap facilities or laboratories of a different kind, but including Mocap as a feature such as interactive rehabilitation platform Motek CAREN[2].

Acknowledgments: Grant number goes here - will be provided later.

Author Contributions: P.S. conceived the idea, provided the theory, and prepared the analysis tools; M.P conducted the experiments and performed the computations; both authors analyzed and discussed the concepts and results; both authors wrote the paper.

Conflicts of Interest: The authors declare no conflict of interest.

Abbreviations

The following abbreviations are used in this manuscript:

ACO: ant colony optimization
AVAR: Allan variance
ADEV: Allan deviation
LS: least squares
Mocap: motion capture
OMC: optical motion capture
RMSE: root mean square error
PSD: power spectral density
SA: simulated annealing
SD: standard deviation
WLS: weighted least squares.

Appendix A. Estimated noise coefficients

Allan variance numerical values for noise component parameters, estimated with the procedure described in p. 3.4. Tables A1-A3 demonstrate results for T40, Bonita, and Vantage cameras respectively.

[2] The Computer Assisted Rehabilitation ENvironment – https://www.motekmedical.com/product/caren/

Preprints (www.preprints.org) | NOT PEER-REVIEWED | Posted: 17 September 2019 doi:10.20944/preprints201909.0178.v1

Peer-reviewed version available at Sensors 2019, 19, 4435; doi:10.3390/s19204435

Table A1. Estimated noise parameters of T40 cameras type for 2..10 devices

a) x_1

	h_{-2}	h_{-1}	h_0	h_1	h_2	q_{c1}	T_{c1}	q_{c2}	T_{c2}	q_{c3}	T_3	q_{c4}	T_{c4}
All	1.55e-10	2.37e-13	9.26e-07	1.35e-13	5.59e-106	5.00e-02	1.00e-02	1.33e-02	2.25e-01	2.04e-03	5.89e+00	3.06e-04	2.00e+03
8	2.99e-09	1.33e-12	1.12e-06	2.91e-09	2.01e-15	5.56e-03	1.62e-01	9.80e-03	3.00e-01	1.92e-03	6.36e+00	2.39e-04	2.00e+03
6	2.82e-09	4.50e-12	1.27e-06	5.42e-09	4.54e-136	4.93e-03	5.48e-01	1.21e-02	2.05e-01	2.13e-03	7.03e+00	3.20e-04	2.00e+03
5	1.03e-08	3.62e-12	2.09e-06	9.57e-09	3.92e-226	5.38e-03	5.63e-01	1.43e-02	2.42e-01	3.02e-03	6.30e+00	3.66e-04	2.00e+03
4	3.96e-09	3.24e-12	2.63e-06	1.39e-08	2.40e-16	1.99e-02	1.99e-01	7.45e-03	6.35e-01	3.12e-03	7.22e+00	6.01e-04	2.00e+03
3	9.57e-09	9.04e-12	3.83e-06	9.82e-09	3.15e-32	2.09e-02	1.95e-01	5.62e-03	5.68e-01	4.60e-03	6.57e+00	6.51e-04	1.41e+03
2	7.65e-08	3.26e-18	5.09e-06	4.60e-09	1.96e-21	9.28e-03	4.54e+00	2.46e-02	1.79e-01	7.63e-10	5.74e+01	5.36e-10	1.55e+03

b) y_1

	h_{-2}	h_{-1}	h_0	h_1	h_2	q_{c1}	T_{c1}	q_{c2}	T_{c2}	q_{c3}	T_{c3}	A_s	f_0
All	4.59e-08	6.11e-22	1.40e-06	3.91e-22	1.47e-157	1.58e-02	1.00e-01	4.72e-03	1.00e+00	6.36e-12	6.21e+02	1.75e-03	5.00e-02
8	4.62e-08	2.45e-20	1.29e-06	1.55e-08	3.73e-172	1.41e-02	1.00e-01	3.78e-03	1.93e+00	6.78e-11	6.73e+02	1.22e-03	2.98e-01
6	4.56e-08	3.32e-19	1.72e-06	2.21e-08	6.14e-265	1.71e-02	1.00e-01	4.26e-03	2.72e+00	4.65e-11	3.65e+02	1.75e-03	2.98e-01
5	5.04e-08	1.59e-19	1.73e-06	2.43e-08	1.50e-69	1.76e-02	1.00e-01	4.62e-03	2.70e+00	5.84e-11	8.47e+02	1.72e-03	2.98e-01
4	5.53e-08	3.88e-19	1.58e-06	2.35e-08	2.12e-70	1.99e-02	1.00e-01	5.84e-03	2.54e+00	8.04e-11	6.60e+02	1.51e-03	2.98e-01
3	6.34e-08	5.93e-19	2.06e-06	2.56e-08	8.38e-187	2.03e-02	1.00e-01	5.74e-03	3.62e+00	9.94e-11	3.88e+02	1.38e-03	2.98e-01
2	7.30e-08	1.29e-14	3.58e-08	7.00e-10	1.29e-51	2.91e-01	1.76e-03	8.38e-03	3.72e+00	2.22e-08	9.20e+02	2.99e-03	5.00e-02

c) z_1

	h_{-2}	h_{-1}	h_0	h_1	h_2	q_{c1}	T_{c1}	q_{c2}	T_{c2}	q_{c3}	T_{c3}	q_{c4}	T_{c4}	A_s	f_0
All	3.23e-09	4.20e-12	1.26e-06	1.04e-13	3.12e-198	1.87e-02	1.00e-01	6.76e-03	5.10e-01	1.69e-03	7.75e+00	1.70e-04	4.43e+02	3.56e-03	1.44e+01
8	5.04e-09	3.53e-13	1.83e-06	9.68e-09	1.36e-105	3.15e-06	5.29e-02	1.23e-02	3.22e-01	2.29e-03	7.66e+00	2.48e-04	6.75e+02	4.19e-03	1.44e+01
6	2.00e-08	8.84e-19	4.33e-06	2.72e-08	1.16e-21	5.48e-08	7.75e-02	2.11e-02	2.95e-01	4.17e-03	5.20e+00	7.09e-11	3.98e+02	6.69e-03	1.44e+01
5	4.22e-08	1.61e-19	4.71e-06	4.26e-08	4.48e-22	2.31e-08	2.61e-02	2.32e-02	2.74e-01	5.26e-03	4.24e+00	7.81e-11	7.27e+02	5.30e-03	1.44e+01
4	4.40e-08	1.18e-09	4.49e-06	4.44e-08	2.16e-30	2.06e-02	9.77e-02	2.30e-02	3.06e-01	5.31e-03	4.38e+00	6.32e-07	4.34e+02	1.69e-01	2.21e+04
3	4.39e-08	3.06e-16	7.38e-06	3.40e-08	2.34e-47	1.57e-05	1.44e-02	2.91e-02	2.19e-01	6.44e-03	5.22e+00	3.55e-04	1.00e+03	4.31e-01	1.03e+18
2	1.39e-07	1.44e-15	6.49e-06	6.02e-08	2.54e-114	6.43e-07	8.02e-02	3.32e-02	1.53e-01	1.33e-02	3.87e+00	1.19e-08	5.01e+02	6.25e-03	1.41e+01

d) x_2

	h_{-2}	h_{-1}	h_0	h_1	h_2	q_{c1}	T_{c1}	q_{c2}	T_{c2}	q_{c3}	T_3	q_{c4}	T_{c4}
All	3.87e-09	2.76e-49	1.13e-06	1.48e-49	1.15e-233	1.16e-02	1.20e-01	7.82e-03	3.20e-01	1.84e-03	6.67e+00	1.58e-04	2.00e+03
8	7.28e-09	5.06e-13	1.21e-06	3.81e-09	7.99e-16	8.67e-03	2.00e-01	7.56e-03	3.00e-01	2.11e-03	5.85e+00	2.68e-07	6.23e+02
6	8.11e-09	4.65e-12	1.40e-06	5.46e-09	1.46e-14	1.17e-02	1.95e-01	6.44e-03	3.68e-01	2.34e-03	6.27e+00	8.61e-05	2.00e+03
5	1.28e-08	6.62e-13	1.89e-06	9.90e-09	7.36e-175	1.36e-02	2.00e-01	7.82e-03	4.21e-01	3.06e-03	5.69e+00	2.65e-04	2.00e+03
4	1.06e-08	7.01e-13	2.36e-06	9.55e-09	6.19e-43	2.02e-02	1.94e-01	7.42e-03	5.61e-01	3.27e-03	6.42e+00	4.45e-04	2.00e+03
3	5.84e-14	1.90e-13	4.40e-06	5.61e-09	1.75e-50	2.38e-02	1.79e-01	7.00e-03	6.40e-01	4.99e-03	6.26e+00	7.95e-04	1.59e+03
2	1.17e-07	6.66e-18	6.11e-06	2.10e-17	1.25e-33	2.83e-02	1.85e-01	2.75e-03	8.07e-01	1.12e-02	4.24e+00	1.54e-10	1.25e+03

e) y_2

	h_{-2}	h_{-1}	h_0	h_1	h_2	q_{c1}	T_{c1}	q_{c2}	T_{c2}	q_{c3}	T_{c3}	A_s	f_0
All	4.60e-08	1.19e-22	1.29e-06	2.56e-23	1.83e-163	1.55e-02	1.00e-01	4.85e-03	1.00e+00	1.78e-12	6.32e+02	1.34e-03	3.69e-02
8	4.87e-08	2.22e-20	9.29e-07	1.79e-08	3.87e-23	1.55e-02	1.00e-01	4.86e-03	1.37e+00	3.11e-13	5.27e+01	3.82e-03	1.37e+01
6	4.97e-08	4.97e-22	1.69e-06	1.10e-08	9.16e-25	1.68e-02	1.00e-01	6.71e-03	1.00e+00	1.71e-12	4.53e+02	2.51e-03	2.68e-02
5	6.18e-08	3.91e-21	1.99e-06	1.49e-08	4.88e-23	1.76e-02	1.00e-01	7.23e-03	1.03e+00	7.33e-11	1.42e+03	3.50e-03	2.35e-02
4	7.04e-08	1.11e-19	1.62e-06	1.40e-08	8.68e-23	2.07e-02	1.00e-01	7.57e-03	1.45e+00	5.02e-11	5.73e+02	3.77e-03	2.40e-02
3	7.77e-08	1.15e-18	1.67e-06	2.28e-08	2.64e-309	2.12e-02	1.00e-01	7.22e-03	3.65e+00	1.15e-10	1.20e+03	3.66e-03	1.41e+01
2	9.83e-08	5.57e-12	8.11e-09	3.93e-09	1.25e-15	2.75e-01	2.30e-03	9.90e-03	2.74e+00	6.15e-07	9.29e+02	6.39e-03	1.95e-02

f) z_2

	h_{-2}	h_{-1}	h_0	h_1	h_2	q_{c1}	T_{c1}	q_{c2}	T_{c2}	q_{c3}	T_{c3}	q_{c4}	T_{c4}	A_s	f_0
All	6.01e-09	2.51e-19	1.11e-06	1.10e-19	1.56e-25	7.49e-02	1.00e-02	1.56e-02	1.98e-01	2.20e-03	5.61e+00	5.15e-11	4.07e+02	1.08e-03	1.70e-01
8	1.13e-08	1.98e-18	2.22e-06	1.29e-09	2.76e-21	5.57e-08	1.03e-02	1.31e-02	2.67e-01	2.63e-03	6.34e+00	1.09e-10	2.01e+02	1.11e-03	1.81e-01
6	2.68e-08	5.11e-19	4.83e-06	4.89e-09	6.68e-117	2.57e-08	2.65e-02	2.16e-02	2.52e-01	4.65e-03	3.95e+00	5.00e-11	3.20e+02	1.50e-03	1.92e-01
5	4.92e-08	3.92e-20	5.20e-06	2.41e-08	2.20e-55	3.60e-08	2.53e-02	2.26e-02	2.38e-01	5.64e-03	4.02e+00	3.51e-11	3.69e+02	2.01e-03	2.63e-01
4	5.09e-08	7.10e-19	4.83e-06	1.95e-08	1.63e-82	9.90e-08	1.67e-02	2.76e-02	2.21e-01	5.93e-03	3.81e+00	1.57e-10	8.56e+02	1.93e-03	2.17e-01
3	7.67e-08	7.72e-19	7.65e-06	2.43e-08	4.60e-21	1.12e-08	8.42e-02	3.15e-02	1.71e-01	7.61e-03	4.47e+00	1.30e-10	5.86e+02	2.28e-03	3.83e-01
2	2.14e-07	8.77e-18	9.50e-06	1.65e-08	8.49e-49	3.99e-08	5.36e-02	3.34e-02	1.65e-01	1.52e-02	3.96e+00	6.98e-10	1.16e+02	5.07e-09	3.21e-01

g) distance - L

	h_{-2}	h_{-1}	h_0	h_1	h_2	q_{c1}	T_{c1}	q_{c2}	T_{c2}	q_{c3}	T_3	q_{c4}	T_{c4}	A_s	f_0
All	1.11e-09	3.69e-16	2.13e-06	3.64e-17	1.37e-20	1.63e-02	1.63e-01	1.77e-03	4.95e+00	2.78e-04	2.18e+02	6.50e-10	7.88e+02	1.56e-03	3.14e+00
8	1.28e-09	2.73e-16	2.21e-06	8.55e-09	1.08e-64	1.32e-02	2.20e-01	1.84e-03	5.04e+00	1.30e-08	1.93e+02	3.28e-04	2.20e+02	1.81e-03	1.44e+01
6	1.48e-09	4.97e-10	2.87e-06	1.05e-08	2.48e-114	1.55e-02	2.15e-01	2.02e-03	5.35e+00	2.95e-04	2.24e+02	2.22e-04	2.27e+02	9.97e-01	5.59e+06
5	8.19e-10	8.50e-17	4.42e-06	2.08e-08	7.00e-19	1.88e-02	2.29e-01	2.48e-03	3.67e+00	4.52e-04	3.06e+02	9.20e-09	2.26e+03	7.95e-01	8.45e+37
4	1.17e-09	8.99e-10	5.59e-06	1.66e-08	5.18e-294	2.46e-02	2.12e-01	2.73e-03	3.71e+00	7.55e-05	3.32e+02	4.53e-04	3.32e+02	7.65e-01	1.91e+04
3	5.57e-09	1.19e-09	1.03e-05	8.12e-10	2.96e-52	2.80e-02	2.19e-01	4.20e-03	4.67e+00	2.29e-04	9.60e+02	3.80e-04	1.11e+03	7.18e-01	6.24e+03
2	9.01e-09	1.14e-11	1.73e-05	1.54e-08	1.21e-36	3.86e-02	2.30e-01	9.01e-03	4.29e+00	2.99e-06	5.32e+02	8.25e-04	1.94e+03	5.27e-02	6.47e+27

Appendix B. Supplementary measurement Allan deviation

For the verification, because of the camera failure, we repeated the testing steady sequence capture after replacing the failing camera. In Fig. A1 we demonstrate 'z' dimension of M1 marker for maximal numbers (10) of each camera type and all the cameras together. We could observe that short term correlated noises disappeared, whereas the bumps representing periodic and long-term correlated noises remain.

Bibliography

1. Szczęsna, A.; Skurowski, P.; Pruszowski, P.; Pęszor, D.; Paszkuta, M.; Wojciechowski, K. Reference Data Set for Accuracy Evaluation of Orientation Estimation Algorithms for Inertial Motion Capture Systems.

Preprints (www.preprints.org) | NOT PEER-REVIEWED | Posted: 17 September 2019 doi:10.20944/preprints201909.0178.v1

Peer-reviewed version available at Sensors 2019, 19, 4435; doi:10.3390/s19204435

Table A2. Estimated noise parameters of Bonita cameras type for 2..10 devices

a) x_1

	h_{-2}	h_{-1}	h_0	h_1	h_2	q_{c1}	T_{c1}	q_{c2}	T_{c2}	q_{c3}	T_3
All	1.51e-07	5.10e-14	1.08e-04	4.69e-07	9.44e-24	2.03e-01	4.23e-02	8.49e-07	4.32e+02	5.23e-03	5.84e+02
8	4.22e-07	6.06e-14	2.57e-04	4.45e-15	7.44e-154	8.85e-02	1.24e-01	1.43e-06	2.88e+02	6.70e-03	3.63e+02
6	6.41e-07	3.29e-13	2.79e-04	1.87e-14	1.63e-16	7.32e-02	1.78e-01	3.56e-04	3.66e+02	8.14e-03	3.66e+02
5	1.73e-06	2.04e-06	4.87e-04	1.92e-14	1.63e-74	4.14e-02	1.11e+00	1.25e-02	3.32e+02	3.48e-06	4.75e+02
4	2.15e-06	1.44e-14	7.99e-04	5.05e-14	1.11e-16	6.25e-02	4.36e-01	1.40e-05	3.46e+02	1.35e-02	3.41e+02
3	8.61e-06	1.74e-04	3.22e-03	4.35e-15	1.68e-70	3.23e-01	1.00e-01	6.61e-06	2.56e+02	3.23e-02	2.84e+02
2	4.81e-06	8.80e-05	2.09e-03	8.38e-19	4.38e-52	2.74e-01	1.00e-01	3.18e-05	2.90e+02	2.59e-02	2.81e+02

b) y_1

	h_{-2}	h_{-1}	h_0	h_1	h_2	q_{c1}	T_{c1}	q_{c2}	T_{c2}	q_{c3}	T_3
All	3.05e-07	3.40e-15	5.03e-05	5.84e-08	1.16e-34	6.69e-02	4.23e-02	8.00e-03	1.00e+00	1.89e-03	2.80e+02
8	5.37e-07	1.13e-12	5.22e-05	8.25e-07	3.69e-15	4.38e-01	1.05e-02	1.14e-02	1.27e+00	2.08e-03	2.13e+02
6	5.89e-07	1.64e-14	7.07e-05	3.66e-07	6.40e-15	2.39e-01	1.53e-02	1.43e-02	1.43e+00	3.84e-03	2.13e+02
5	3.05e-07	1.87e-14	1.10e-04	1.24e-13	3.13e-73	7.00e-02	1.00e-02	2.04e-02	1.96e+00	7.53e-03	2.39e+02
4	1.52e-06	2.15e-14	1.15e-04	1.73e-06	4.07e-16	7.00e-01	1.00e-02	2.75e-02	1.75e+00	8.78e-03	2.19e+02
3	1.67e-06	4.26e-12	6.83e-04	2.03e-12	1.82e-15	1.00e+00	1.44e-02	3.97e-02	1.26e+00	2.01e-02	3.82e+02
2	3.83e-06	1.16e-12	1.04e-03	2.15e-13	1.69e-31	1.00e+00	1.89e-02	3.84e-02	1.30e+00	2.08e-02	3.72e+02

c) z_1

	h_{-2}	h_{-1}	h_0	h_1	h_2	q_{c1}	T_{c1}	q_{c2}	T_{c2}	q_{c3}	T_3	q_{c4}	T_{c4}
All	1.58e-07	1.14e-14	8.87e-05	2.07e-14	2.67e-231	1.12e-01	6.35e-02	7.39e-08	2.01e+00	2.59e-05	4.44e+02	4.81e-03	4.44e+02
8	2.24e-07	5.38e-13	1.37e-04	3.07e-07	4.51e-135	1.82e-01	3.85e-02	1.50e-02	1.00e+00	5.96e-03	3.46e+02	2.46e-07	1.39e+03
6	1.79e-07	5.87e-14	7.45e-05	1.30e-13	1.02e-53	9.75e-02	7.88e-02	1.40e-07	4.62e+00	1.01e-03	5.00e+02	4.86e-03	5.00e+02
5	2.14e-07	1.81e-14	8.08e-05	4.81e-14	1.17e-16	1.13e-01	6.13e-02	3.04e-03	1.00e+00	2.75e-07	2.72e+02	5.66e-03	3.04e+02
4	8.68e-07	1.47e-14	1.47e-04	1.39e-13	1.26e-75	1.68e-01	4.97e-02	1.40e-02	1.00e+00	6.90e-06	3.58e+02	8.86e-03	3.41e+02
3	1.11e-06	5.33e-19	4.60e-04	7.17e-18	4.83e-55	1.00e+00	1.74e-02	4.29e-07	3.33e+00	3.79e-06	3.46e+02	1.15e-02	3.42e+02
2	1.63e-06	2.21e-13	8.59e-04	1.76e-13	1.46e-124	1.00e+00	1.91e-02	2.25e-07	3.42e+00	1.18e-06	9.87e+02	1.49e-02	3.08e+02

d) x_2

	h_{-2}	h_{-1}	h_0	h_1	h_2	q_{c1}	T_{c1}	q_{c2}	T_{c2}	q_{c3}	T_3
All	2.84e-08	1.72e-15	3.75e-05	4.99e-16	6.55e-278	6.39e-02	9.30e-02	2.06e-07	1.96e+02	3.80e-03	2.89e+02
8	2.60e-08	2.22e-21	6.59e-05	2.49e-17	5.03e-136	8.46e-02	9.43e-02	5.75e-07	1.93e+02	5.32e-03	2.34e+02
6	1.26e-07	2.89e-06	9.24e-05	6.32e-17	7.76e-23	1.01e-01	1.18e-01	5.15e-06	1.86e+02	7.25e-03	1.82e+02
5	2.56e-07	5.80e-16	8.06e-05	3.26e-13	2.45e-10	2.02e-01	4.48e-02	4.89e-08	1.96e+02	3.50e-03	2.22e+02
4	2.28e-07	1.87e-13	1.97e-04	1.48e-15	1.24e-29	1.48e-01	1.07e-01	2.77e-07	1.78e+02	9.28e-03	1.85e+02
3	2.84e-07	3.01e-04	7.19e-04	1.58e-12	2.72e-20	4.52e-01	5.79e-02	3.65e-02	5.95e+01	7.31e-03	9.28e+02
2	1.23e-06	7.34e-04	7.60e-04	3.99e-06	9.54e-48	7.65e-01	2.94e-02	6.96e-02	3.21e+01	1.87e-02	2.63e+02

e) y_2

	h_{-2}	h_{-1}	h_0	h_1	h_2	q_{c1}	T_{c1}	q_{c2}	T_{c2}	q_{c3}	T_3
All	2.49e-07	8.04e-16	2.97e-05	1.15e-16	9.63e-203	6.98e-02	9.21e-02	4.87e-03	5.87e+01	6.49e-10	7.55e+02
8	3.58e-07	1.49e-15	4.00e-05	5.21e-17	1.23e-19	6.87e-02	9.73e-02	3.83e-03	5.96e+01	1.26e-09	5.54e+02
6	3.55e-07	3.23e-16	6.27e-05	8.38e-17	1.34e-84	1.01e-01	9.35e-02	7.53e-03	5.43e+01	1.51e-08	6.63e+02
5	6.67e-08	7.32e-35	4.09e-05	4.11e-14	8.14e-56	9.46e-02	5.76e-02	2.30e-07	2.40e+02	2.46e-03	8.78e+02
4	4.91e-07	1.26e-15	9.85e-05	4.51e-17	1.74e-80	1.39e-01	8.15e-02	7.58e-03	6.38e+01	4.36e-09	4.58e+02
3	1.17e-07	2.90e-13	2.36e-04	8.80e-14	2.58e-64	2.10e-01	8.00e-02	1.28e-02	6.35e+01	2.52e-03	1.00e+03
2	2.75e-07	5.17e-05	3.92e-04	4.11e-13	1.22e-16	2.50e-01	7.43e-02	2.18e-02	5.30e+01	3.78e-03	6.58e+02

f) z_2

	h_{-2}	h_{-1}	h_0	h_1	h_2	q_{c1}	T_{c1}	q_{c2}	T_{c2}	q_{c3}	T_3	q_{c4}	T_{c4}
All	1.09e-07	2.60e-16	2.66e-05	5.01e-15	1.27e-17	6.71e-02	7.44e-02	1.92e-08	3.79e+00	2.06e-07	3.26e+02	4.26e-03	2.72e+02
8	7.80e-08	4.66e-16	4.29e-05	2.39e-14	6.73e-17	8.26e-02	6.47e-02	9.21e-08	1.90e+00	5.16e-07	2.99e+02	4.56e-03	3.49e+02
6	9.31e-08	8.69e-32	3.32e-05	8.88e-19	1.54e-41	5.64e-02	8.44e-02	1.41e-07	2.41e+00	3.86e-07	3.71e+02	3.98e-03	3.56e+02
5	1.25e-17	5.20e-14	2.47e-05	3.35e-07	1.92e-15	1.90e-01	2.02e-02	2.22e-07	2.62e+00	6.31e-07	9.16e+02	2.85e-03	1.39e+03
4	2.27e-07	1.22e-27	6.65e-05	7.89e-08	2.24e-16	8.96e-02	6.13e-02	1.72e-08	6.01e+00	4.84e-03	2.41e+02	8.49e-08	1.32e+03
3	3.29e-07	2.29e-14	2.18e-04	1.37e-14	1.90e-17	1.06e-01	1.26e-01	1.84e-07	2.95e+00	1.04e-07	3.77e+01	9.09e-03	1.83e+02
2	5.91e-07	6.08e-12	4.52e-04	5.51e-13	1.14e-80	1.93e-01	9.98e-02	1.97e-02	1.00e+00	6.15e-03	2.67e+02	1.72e-02	1.00e+02

g) distance - L

	h_{-2}	h_{-1}	h_0	h_1	h_2	q_{c1}	T_{c1}	q_{c2}	T_{c2}	q_{c3}	T_3
All	3.66e-07	1.07e-14	1.42e-04	9.68e-07	1.64e-57	2.71e-01	3.80e-02	3.60e-06	5.77e+02	4.54e-03	6.29e+02
8	4.76e-07	1.65e-14	3.66e-04	6.23e-07	7.35e-134	2.54e-01	4.96e-02	6.34e-08	7.52e+02	5.71e-03	5.66e+02
6	8.36e-07	2.17e-14	4.73e-04	4.08e-14	1.44e-281	2.32e-01	7.01e-02	4.49e-07	6.75e+02	7.86e-03	3.67e+02
5	1.67e-06	6.51e-13	1.09e-03	9.42e-14	8.56e-85	1.23e-01	1.65e-01	1.35e-06	4.90e+02	1.09e-02	3.77e+02
4	2.13e-06	7.89e-14	1.29e-03	4.91e-13	7.31e-101	3.31e-01	7.02e-02	9.45e-06	5.40e+02	1.21e-02	5.22e+02
3	1.78e-05	2.76e-04	4.52e-03	2.25e-14	5.49e-79	1.00e+00	4.68e-02	3.76e-02	8.31e+01	2.27e-02	2.00e+02
2	1.10e-05	4.28e-04	4.09e-03	1.84e-13	1.29e-38	1.00e+00	4.81e-02	6.18e-02	2.92e+01	3.17e-02	2.00e+02

In Computer Vision and Graphics; Chmielewski, L.J.; Datta, A.; Kozera, R.; Wojciechowski, K., Eds.; Springer International Publishing: Cham, 2016; Vol. 9972, LNCS, pp. 509–520.

2. Szczęsna, A.; Skurowski, P.; Lach, E.; Pruszowski, P.; Pęszor, D.; Paszkuta, M.; Słupik, J.; Lebek, K.; Janiak, M.; Polański, A.; Wojciechowski, K. Inertial Motion Capture Costume Design Study. Sensors **2017**, 17, 612.
3. Nichols, J.K.; Sena, M.P.; Hu, J.L.; O'Reilly, O.M.; Feeley, B.T.; Lotz, J.C. A Kinect-based movement assessment system: marker position comparison to Vicon. Computer Methods in Biomechanics and Biomedical Engineering **2017**, 20, 1289–1298.
4. Al-Amri, M.; Nicholas, K.; Button, K.; Sparkes, V.; Sheeran, L.; Davies, J.L. Inertial Measurement Units for Clinical Movement Analysis: Reliability and Concurrent Validity. Sensors **2018**, 18, 719.

Table A3. Estimated noise parameters of Vantage cameras type for 2..9 devices

a) x_1

	h_{-2}	h_{-1}	h_0	h_1	h_2	q_{c1}	T_{c1}	q_{c2}	T_{c2}	q_{c3}	T_3
All	6.91e-08	7.58e-14	3.21e-05	2.33e-12	2.26e-10	6.88e-02	6.10e-02	5.97e-08	5.30e+01	6.38e-04	2.00e+03
9	1.68e-08	9.54e-07	2.64e-05	1.05e-10	1.98e-10	4.00e-02	5.94e-02	1.05e-03	1.47e+01	8.34e-04	2.51e+02
8	1.33e-17	1.40e-13	1.39e-05	8.82e-13	6.45e-11	1.92e-02	9.99e-02	1.51e-03	9.34e+00	1.36e-03	8.02e+02
6	2.38e-08	2.39e-11	3.70e-05	2.41e-11	2.38e-10	3.78e-02	6.77e-02	1.51e-03	6.57e+00	8.53e-04	2.71e+02
5	4.34e-08	8.09e-07	4.65e-05	1.66e-10	3.94e-10	5.37e-02	5.18e-02	1.28e-03	8.20e+00	6.46e-04	1.10e+03
4	1.11e-08	3.70e-06	2.51e-05	1.64e-07	2.28e-189	3.79e-01	1.59e-02	1.81e-03	7.49e+00	1.35e-03	8.45e+02
3	1.66e-06	6.36e-20	1.17e-04	3.86e-07	1.13e-21	1.39e-02	1.13e-01	7.65e-11	1.84e+01	4.92e-03	4.07e+00
2	1.22e-06	3.07e-20	4.51e-04	3.50e-06	1.77e-77	7.21e-08	1.15e-02	2.23e-02	1.80e+00	2.28e-11	1.09e+03

b) y_1

	h_{-2}	h_{-1}	h_0	h_1	h_2	q_{c1}	T_{c1}	q_{c2}	T_{c2}	q_{c3}	T_3
All	3.30e-07	6.68e-13	4.46e-05	1.52e-06	2.29e-14	1.89e-01	2.50e-02	1.38e-07	8.61e+01	6.44e-08	1.78e+03
9	3.04e-07	1.53e-21	3.04e-05	1.74e-20	3.43e-10	3.21e-02	8.13e-02	1.69e-11	7.71e+01	1.74e-11	1.81e+03
8	3.43e-07	1.22e-19	1.17e-05	1.29e-07	7.44e-11	5.81e-03	6.82e-01	6.01e-11	6.48e+01	4.49e-12	1.45e+03
6	3.87e-07	1.13e-19	3.63e-05	9.38e-07	6.77e-18	1.74e-01	1.91e-02	4.16e-09	3.93e+01	7.51e-08	7.81e+02
5	3.53e-07	1.38e-21	2.76e-05	9.58e-07	2.70e-126	2.18e-01	1.69e-02	1.72e-11	5.26e+01	1.69e-11	1.46e+03
4	5.25e-07	1.10e-19	1.30e-05	5.23e-07	5.64e-21	3.29e-01	1.00e-02	1.69e-10	6.65e+01	5.12e-11	1.70e+03
3	1.69e-14	1.79e-14	1.84e-04	5.32e-07	3.87e-108	1.38e-04	1.39e-02	4.97e-03	7.88e+00	6.51e-03	1.66e+03
2	1.55e-06	5.81e-13	5.79e-03	4.74e-11	2.05e-08	2.86e-02	1.00e+00	1.16e-02	5.00e+00	6.45e-03	2.00e+03

c) z_1

	h_{-2}	h_{-1}	h_0	h_1	h_2	q_{c1}	T_{c1}	q_{c2}	T_{c2}	q_{c3}	T_3
All	5.06e-08	7.72e-06	1.96e-04	1.28e-06	1.12e-09	1.83e-01	3.52e-02	3.07e-03	1.38e+01	1.69e-03	3.83e+02
9	5.72e-08	7.29e-14	1.01e-04	1.95e-15	1.19e-41	8.53e-03	2.41e+00	2.84e-03	1.39e+01	1.95e-03	2.42e+02
8	7.38e-27	5.85e-13	2.86e-05	4.07e-17	3.49e-55	1.88e-02	2.14e-01	2.67e-03	1.00e+01	2.33e-03	9.33e+02
6	1.40e-07	4.95e-14	2.30e-04	7.33e-07	4.49e-17	1.65e-02	1.00e+00	7.43e-03	1.00e+01	2.47e-03	4.33e+02
5	1.06e-07	2.03e-15	2.17e-04	3.22e-13	2.91e-10	1.21e-02	3.05e+00	4.15e-03	1.00e+01	2.88e-03	1.73e+02
4	3.31e-07	6.65e-20	7.48e-05	8.79e-08	6.94e-119	3.08e-07	1.63e-02	4.30e-03	1.83e+01	5.64e-10	1.78e+03
3	2.02e-06	5.51e-18	4.43e-04	2.32e-06	4.04e-21	2.87e-02	1.66e-01	9.05e-03	1.58e+01	2.75e-10	1.18e+03
2	9.78e-07	4.27e-13	2.75e-03	2.01e-06	1.85e-08	1.44e-02	7.88e-01	1.09e-02	1.00e+01	3.09e-03	2.00e+03

d) x_2

	h_{-2}	h_{-1}	h_0	h_1	h_2	q_{c1}	T_{c1}	q_{c2}	T_{c2}	q_{c3}	T_3
All	3.57e-07	1.72e-18	2.09e-05	8.51e-07	2.86e-20	2.88e-01	4.36e-02	4.83e-03	5.00e+00	2.06e-10	7.50e+02
9	7.36e-08	2.58e-06	1.38e-05	5.75e-08	5.97e-11	6.82e-02	2.91e-02	1.36e-03	6.69e+01	1.45e-03	1.00e+01
8	7.30e-08	7.31e-16	2.34e-05	7.52e-08	8.97e-18	5.39e-03	5.85e-01	2.28e-03	1.70e+01	6.37e-04	2.27e+02
6	5.07e-08	3.29e-06	2.33e-05	2.94e-07	6.57e-40	1.34e-01	2.01e-02	1.87e-03	1.09e+01	1.39e-03	1.27e+02
5	1.78e-08	3.14e-06	1.58e-05	3.45e-07	1.01e-14	1.48e-01	2.34e-02	2.97e-07	7.45e+01	2.26e-03	1.20e+02
4	7.76e-08	1.07e-21	3.25e-05	1.32e-07	2.32e-45	2.75e-03	7.26e-01	1.56e-03	5.00e+00	6.04e-12	3.52e+02
3	1.11e-06	1.02e-19	1.05e-04	8.44e-07	1.49e-70	3.31e-02	6.01e-02	4.51e-03	1.12e+01	4.19e-10	6.47e+02
2	1.01e-06	1.91e-11	1.06e-04	9.24e-07	1.54e-13	4.17e-02	4.87e-02	4.55e-03	1.23e+01	1.60e-03	1.00e+03

e) y_2

	h_{-2}	h_{-1}	h_0	h_1	h_2	q_{c1}	T_{c1}	q_{c2}	T_{c2}	q_{c3}	T_3
All	7.00e-07	7.81e-20	3.31e-05	1.10e-06	8.52e-24	3.27e-01	4.45e-02	5.71e-03	1.00e+00	4.57e-11	7.57e+02
9	2.87e-07	5.04e-22	1.73e-05	1.23e-07	1.67e-39	1.48e-02	1.04e-01	1.10e-11	5.71e+01	8.10e-12	5.13e+02
8	3.00e-07	1.20e-21	1.87e-05	1.80e-07	4.97e-52	9.22e-03	1.78e-01	9.94e-12	6.08e+01	1.08e-12	1.16e+03
6	5.70e-07	1.77e-21	5.10e-05	3.32e-07	4.11e-23	1.63e-02	1.24e-01	1.84e-11	3.15e+01	1.84e-11	4.73e+02
5	6.18e-07	1.18e-21	5.69e-05	2.54e-07	1.94e-22	2.13e-02	1.18e-01	1.75e-11	3.72e+01	2.41e-12	1.52e+03
4	7.42e-07	3.67e-22	5.73e-05	4.83e-07	5.82e-23	6.66e-03	1.40e-01	1.49e-11	6.75e+01	2.22e-12	9.24e+02
3	3.43e-14	7.65e-13	1.48e-04	1.29e-06	5.13e-42	9.16e-02	2.34e-02	4.17e-03	1.22e+01	5.63e-03	1.50e+03
2	1.56e-55	3.38e-12	1.51e-04	1.34e-06	2.72e-14	6.62e-02	3.32e-02	4.05e-03	1.07e+01	5.59e-03	1.84e+03

f) z_2

	h_{-2}	h_{-1}	h_0	h_1	h_2	q_{c1}	T_{c1}	q_{c2}	T_{c2}	q_{c3}	T_3
All	8.45e-07	1.28e-17	4.79e-05	2.33e-06	1.28e-20	4.92e-01	4.36e-02	8.16e-03	5.60e+00	4.33e-10	1.57e+02
9	1.58e-08	1.06e-13	3.09e-05	9.29e-13	1.17e-10	1.18e-02	2.09e-01	2.35e-03	1.55e+01	2.00e-03	3.84e+02
8	6.99e-08	1.04e-13	3.99e-05	3.74e-07	1.68e-69	9.82e-03	2.64e-01	3.00e-03	2.49e+01	1.54e-03	4.91e+02
6	1.93e-07	4.51e-15	8.39e-05	4.72e-07	5.47e-17	2.16e-02	1.30e-01	3.59e-03	2.99e+01	2.02e-03	3.06e+02
5	9.92e-08	5.29e-14	7.82e-05	3.02e-07	3.46e-16	1.85e-02	1.63e-01	3.35e-03	2.30e+01	2.61e-03	3.95e+02
4	4.74e-07	2.78e-14	8.11e-05	7.05e-07	2.31e-16	5.26e-03	1.21e-01	3.92e-03	2.74e+01	1.04e-03	1.00e+03
3	6.74e-07	1.33e-15	3.74e-04	3.40e-06	1.25e-121	5.36e-02	6.81e-02	5.85e-03	1.34e+01	5.67e-03	9.60e+01
2	6.99e-07	2.22e-16	3.73e-04	3.39e-06	1.27e-152	5.42e-02	6.73e-02	5.85e-03	1.39e+01	5.69e-03	9.69e+01

g) distance - L

	h_{-2}	h_{-1}	h_0	h_1	h_2	q_{c1}	T_{c1}	q_{c2}	T_{c2}	q_{c3}	T_3
All	3.29e-07	5.09e-16	6.21e-05	1.55e-06	3.77e-213	3.32e-01	4.36e-02	4.34e-03	5.00e+00	1.71e-09	8.56e+02
9	5.83e-08	4.58e-06	5.03e-05	3.87e-07	6.34e-130	1.07e-01	3.73e-02	2.11e-06	4.63e+01	1.38e-03	6.08e+01
8	4.45e-08	5.56e-17	4.01e-05	7.38e-30	4.85e-88	6.96e-03	7.22e-01	1.20e-03	5.00e+00	2.27e-04	1.00e+03
6	9.82e-08	3.03e-06	7.73e-05	1.88e-11	6.89e-10	9.39e-02	4.76e-02	1.89e-03	2.42e+01	8.69e-08	4.44e+02
5	9.48e-08	9.21e-06	7.92e-05	9.95e-07	1.15e-24	2.08e-01	2.61e-02	1.25e-03	4.27e+01	1.79e-03	5.00e+01
4	1.06e-07	2.94e-15	7.27e-05	3.30e-15	4.33e-18	2.29e-01	2.73e-02	2.37e-03	5.00e+00	2.67e-10	5.67e+02
3	1.93e-07	7.36e-22	2.37e-04	1.02e-06	4.67e-69	1.74e-02	5.80e-01	1.75e-11	1.03e+01	1.14e-11	6.74e+02
2	6.10e-07	4.04e-15	7.92e-04	3.49e-06	1.71e-12	1.21e-02	1.00e+00	6.69e-03	7.37e+00	4.62e-03	1.26e+02

5. Michalczuk, A.; Pęszor, D.; Josiński, H.; Świtoński, A.; Mucha, R.; Wojciechowski, K. Precision of Gait Indices Approximation by Kinect Based Motion Acquisition. New Trends in Intelligent Information and Database Systems; Barbucha, D.; Nguyen, N.T.; Batubara, J., Eds. Springer International Publishing, 2015, Studies in Computational Intelligence, pp. 53–60.
6. Lamine, H.; Bennour, S.; Laribi, M.; Romdhane, L.; Zaghloul, S. Evaluation of Calibrated Kinect Gait Kinematics Using a Vicon Motion Capture System. Computer Methods in Biomechanics and Biomedical Engineering **2017**, 20, 111–112.

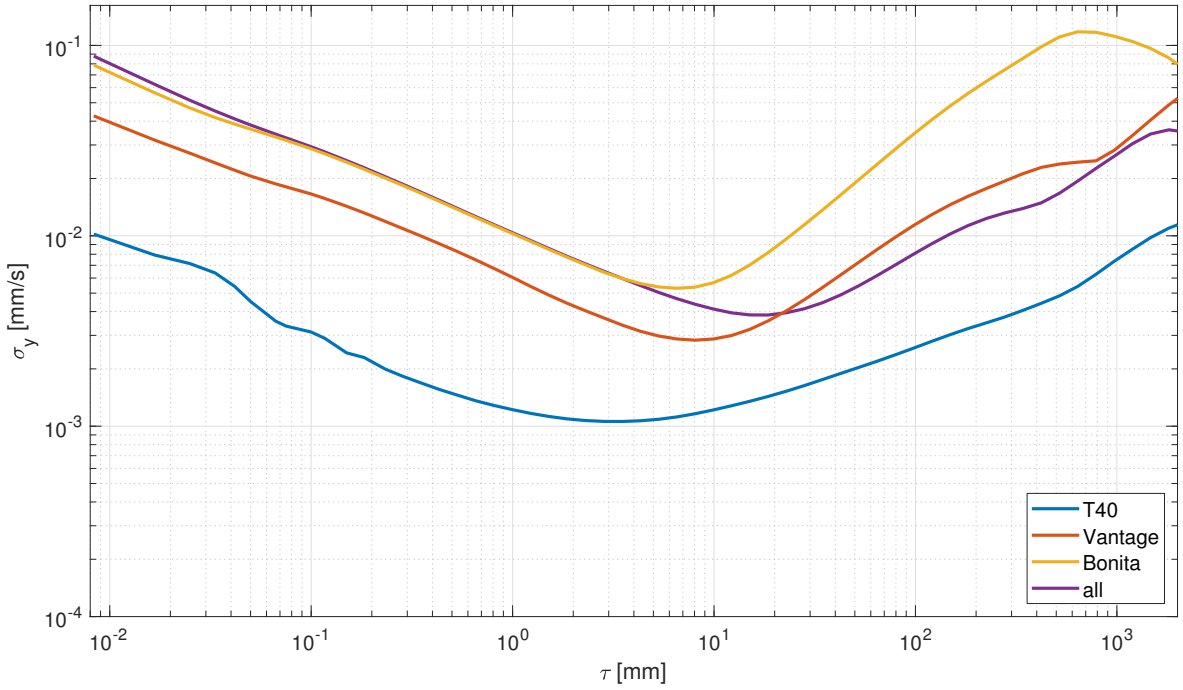

Figure A1. Exemplary Allan deviation for supplementary recording – z_1

7. Kobrick, R.; Carr, C.; Meyen, F.; R Domingues, A.; Dava, P.; Newman, J.; E Jacobs, S. Using Inertial Measurement Units for Measuring Spacesuit Mobility and Work Envelope Capability for Intravehicular and Extravehicular Activities. Proceedings of 63rd International Astronautical Congress; , 2012.
8. Allan, D.W. Statistics of atomic frequency standards. Proceedings of the IEEE **1966**, 54, 221–230.
9. Eichelberger, P.; Ferraro, M.; Minder, U.; Denton, T.; Blasimann, A.; Krause, F.; Baur, H. Analysis of accuracy in optical motion capture–A protocol for laboratory setup evaluation. Journal of Biomechanics **2016**, 49, 2085–2088.
10. Windolf, M.; Götzen, N.; Morlock, M. Systematic accuracy and precision analysis of video motion capturing systems—exemplified on the Vicon-460 system. Journal of Biomechanics **2008**, 41, 2776–2780.
11. Carse, B.; Meadows, B.; Bowers, R.; Rowe, P. Affordable clinical gait analysis: An assessment of the marker tracking accuracy of a new low-cost optical 3D motion analysis system. Physiotherapy **2013**, 99, 347–351.
12. Jensenius, A.; Nymoen, K.; Skogstad, S.; Voldsund, A. A Study of the Noise-Level in Two Infrared Marker-Based Motion Capture Systems. Proceedings of the 9th Sound and Music Computing Conference, SMC 2012; , 2012; pp. 258–263.
13. Duane, C.B. Close-range camera calibration. Photogramm. Eng **1971**, 37, 855–866.
14. Abdel-Aziz, Y.; Karara, H.; Hauck, M. Direct linear transformation from comparator coordinates into object space coordinates in close-range photogrammetry. Photogrammetric Engineering & Remote Sensing **2015**, 81, 103–107.
15. Yang, P.F.; Sanno, M.; Brüggemann, G.P.; Rittweger, J. Evaluation of the performance of a motion capture system for small displacement recording and a discussion for its application potential in bone deformation *in vivo* measurements. Proceedings of the Institution of Mechanical Engineers, Part H: Journal of Engineering in Medicine **2012**, 226, 838–847.
16. Merriaux, P.; Dupuis, Y.; Boutteau, R.; Vasseur, P.; Savatier, X. A Study of Vicon System Positioning Performance. Sensors **2017**, 17, 1591.
17. Raghu, S.L.; Kang, C.k.; Whitehead, P.; Takeyama, A.; Conners, R. Static accuracy analysis of Vicon T40s motion capture cameras arranged externally for motion capture in constrained aquatic environments. Journal of Biomechanics **2019**, 89, 139–142.

18. Joint Committee for Guides in Metrology. JCGM 200:2012 International vocabulary of metrology — Basic and general concepts and associated terms (VIM). Technical report, JCGM, 2008.
19. Luo, C.; Casaseca-de-la Higuera, P.; McClean, S.; Parr, G.; Ren, P. Characterization of Received Signal Strength Perturbations Using Allan Variance. IEEE Transactions on Aerospace and Electronic Systems **2018**, 54, 873–889.
20. Czerwinski, F.; Richardson, A.C.; Oddershede, L.B. Quantifying Noise in Optical Tweezers by Allan Variance. Opt. Express **2009**, 17, 13255–13269.
21. IEEE Standard Specification Format Guide and Test Procedure for Single-Axis Interferometric Fiber Optic Gyros. IEEE Std 952-1997 (R2008) **2008**.
22. Skurowski, P.; Paszkuta, M. Automatic IMU sensor characterization using Allan variance plots. American Institute of Physics Conference Series, 2017, Vol. 1863, American Institute of Physics Conference Series, p. 400007.
23. Vernotte, F.; Lantz, E.; Groslambert, J.; Gagnepain, J.J. Oscillator noise analysis: multivariance measurement. IEEE Transactions on Instrumentation and Measurement **1993**, 42, 342–350.
24. Widuch, J.; Klyta, A. A multistart hybrid algorithm to solving the sequential ordering problem. Studia Informatica **2014**, 35, 29–55.
25. Socha, K.; Dorigo, M. Ant colony optimization for continuous domains. European Journal of Operational Research **2008**, 185, 1155–1173.
26. Liu, H.; Shah, S.; Jiang, W. On-line outlier detection and data cleaning. Computers & Chemical Engineering **2004**, 28, 1635–1647.